Fiber Bragg Gratings (FBG) for Force Sensing in Biomechanics Applications

by

Rachaen Mahfuz Huq

Submitted in partial fulfilment of the requirements
for the degree of Master of Applied Science

at

Dalhousie University
Halifax, Nova Scotia
July, 2019

To my family…

Table of Contents

List of Tables

List of Figures

Abstract

Fiber Optic (FO) sensors are robust, cheap, immune to electromagnetic interference (EMI) and compact, resulting in their high usability in harsh environments. Fiber Bragg Grating (FBG) based sensors have emerged as a popular subclass of fiber optic (FO) sensors finding applications in the fields of Structural Health Monitoring (SHM), oil/gas field monitoring . mainly due to its strong sensitivity to strain and easy integration into complex systems. Although FBGs have found industrial applications in several fields, Biomechanics, being a field largely depending on measurement of forces, pressure strain etc. remains widely unexplored and there has been little work on developing FBG based force sensors, e.g. a force platform for application in biomechanics labs. FBGs are not directly sensitive to transverse force, but longitudinal strain. Transverse force can induce strain via a transducer, but it would also induce challenges such as birefringence (peak splitting). Practical limits of fibers e.g. strain tolerance, transducer deformation also put constrains in designing such systems. Hence, a quantitative study was needed in this area. In this thesis, we have quantitatively proved that it is possible to develop an FBG-based force platform despite the challenges. We have derived suitable FBG parameters and simulated a mechanical transducer that would enable us to do so. The contribution of this thesis is mainly twofold; first: the quality of the reflected spectra from an FBG was systematically analyzed with respect to FBG length and modulation depth leading us to find optimum ranges for a biomechanical force sensing application. Second: a simplified Finite Element Method (FEM) model of a force platform is developed and a static analysis is performed to estimate its behavior under realistic range of forces. Results from the FEM simulation were used to simulate the characteristic of the reflected spectra from an FBG with parameters derived from the previous step. Distortion due to transverse force causing birefringence was also analyzed.

List of Abbreviations and Symbols Used

CAE	Computer Aided Engineering
CMT	Coupled Mode Theory
EMI	Electro-magnetic Interference
EV	Electric Vehicle
EVA	Ethylene-Vinyl Acetate
FBG	Fiber Bragg Grating
FEM	Finite Element Method
FO	Fiber Optic
FWHM	Full Width at Half Maximum
MRI	Magnetic Resonance Imaging
RF	Radio Frequency
RI	Refractive Index
SHM	Structural Health Monitoring
λ_B	Reflected Bragg Wavelength
n_{eff}	Effective Refractive Index (RI) at the grating
Λ_0	Grating pitch, or the period of RI modulation
p_e	Photo-elastic coefficient
$\varepsilon(x)$	Strain variation along x
Λ_0	Grating pitch, or the period of RI modulation
$\overline{\delta_{n_{eff}}}$	DC refractive index (RI) change; modulation depth
ν	Fringe visibility ≈ 1
Λ_0	Grating pitch, or the period of RI modulation
$\phi(x)$	Grating chirp
$\delta_{n_{eff}}(x)$	Effective refractive index (RI) change
$\Delta\lambda_{strain}$	Bragg wavelength shift due to strain
λ_B	Original Bragg wavelength

ε	Strain
$R(x)$	Amplitude of the forward propagating mode (Coupled Mode Theory)
$S(x)$	Amplitude of the backward propagating mode
$\hat{\sigma}$	General DC self coupling coefficient
κ	'ac' coupling coefficient between counter propagating modes.
m	Striate visibility
L	Grating length
E_F	Young modulus of the fiber
ν_F	Poisson ratio of the fiber
n_0	Initial effective refractive index
$\sigma_z, \sigma_y, \sigma_z$	Stress components in the subscripted directions.
p_{11}, p_{12}	Pockel's coefficients

Acknowledgments

First, I would like to thank Almighty Allah (swt) for whatever I have achieved so far. Every time I look back at my life's timeline, I feel blessed thinking about how far I have come, via the routes I have taken, and the choices I made. I would also like to thank my parents for always being there.

I would like to thank my supervisor, Dr. Michael Cada for all his support throughout my journey at Dalhousie. Every feedback and advice I have received from Dr. Cada tremendously helped me grow as an engineer, a researcher and an analytical thinker. I still remember they I day he welcomed me to his group when I started my program; now when I look back, I can only see the amount of learning I have accumulated from interacting with him.

I would like to thank Dr. Vincent Sieben, and Dr. Peter Allen for being my thesis committee members. I would also like to thank Dr. Jaromir Pistora for his feedback during the final phase of my work. Their constructive feedback helped me make my thesis better.

I would also like to thank the members of our research group for their feedback in giving my work the shape it has now, especially Kyle, Naser, Deepak, Barbora, and Sabrina. Special thanks goes to Dr. Youqiao Ma, who sparked the motivation for me to go in this research direction through an amazing presentation in our group back in 2018.

I would like to thank the Killam Trusts and the Faculty of Graduate Studies for funding my studies through the Killam Scholarship and the Nova Scotia Graduate Scholarship respectively. I couldn't imagine studying in such an elite institution without the financial support from them. Thank you for giving me the opportunity!

I would like to thank all the friends I have made here in Halifax, who made this journey much more fun than I had expected; especially Mehedi Bhai and Sabrina. I will miss having all those after hour conversations in the department. I would also like to thank our department secretaries Nicole and Rebecca for making the administrative processes a breeze! You guys are the bests!

Finally, I would like to thank my lovely wife Rimi, for always being there for me and making me a better person every day!

Chapter 1
Introduction

Optical fibers are well known to have revolutionized long-distance data communication with unprecedented improvement in data rates which eventually made it the backbone of internet throughout the globe today. However, the potential of fiber optics goes beyond high data rate communication. In the last two decades, researchers around the world have been exploiting the light propagation properties through a variety of optical fibers to sense temperature, strain, pressure and refractive index among others. This is particularly interesting for harsh sensing environments where immunity to high temperature (~1000°C) [1], pressure (~70 MPa) [2] or electromagnetic interference becomes crucial, such as a coal-fired power plants [1], or structural health monitoring in megastructures or even unmanned aircrafts [3]. Another major benefit that makes fiber optic sensing interesting is its ability to operate in low power and low circuit complexity in the sensing end while allowing signal processing to take place at a distance. While the applications of fiber optic (FO) sensors are relatively new in the field of biomedical and biomechanics applications, researchers agree that the technology has great potential to solve many fundamental problems in this field. In this chapter, a brief overview of FO sensors and its classifications are provided. We would also focus our attention to Fiber Bragg Grating (FBG) sensors and its working principles and potential applications. In this chapter, the motivation to work in this area is justified, and the existing problems in this field that requires attention are explained. Then we would pinpoint a research gap that this thesis focuses on. The scientific contribution of this thesis is also outlined at the end of this chapter with a description of the methods and tools used.

1 Background and Motivation

1.1 Fundamental Advantages of Fiber Optic Sensors

What made fiber optic (FO) sensors interesting in the first place was that it offered an “all passive dielectric approach” to sensing which is crucial in various applications such as medicine, where patients are required to be electrically isolated; or in high voltage environments where conductive paths should ideally be eliminated [4]. Unlike electrical sensors which often require a rigorous shielding resulting in an increased size and cost, FO sensors bring about a low maintenance, low cost and compact solution along with immunity to electromagnetic interference and an ability to

withstand high temperature and vibration environments. A large bandwidth of these fibers also make transportation of sensing data much easier to a remote processing location. The major advantages of FO sensors are summarized in Table 1-1.

Table 1-1 Advantages of Fiber Optic Sensors – A Quick Summary

- Entirely dielectric (passive)
- Compact, lightweight, flexible in hard-to-reach places
- Low cost
- High bandwidth, i.e. very fast changes are detectable
- Immunity to shock, vibration, electromagnetic interference, and high temperature
- High Sensitivity
- Ease of multiplexing and transport of data

1.2 Potential of FO Sensors in Solving Today's Problems

Fiber Optic sensors have a strong potential in solving a number of today's problems, such as robust structural health monitoring systems, monitoring environmental parameters (e.g. temperature, humidity) in harsh conditions, accurate monitoring of batteries in electric vehicles, or in a solar cell infrastructure, biomedical monitoring under electrical isolation etc. [5]–[7]. The evolution of FO sensors will be summarized in the following two subsections to give readers an idea about how the field is evolving and what motivates us to work in this direction. This sets a good backdrop before we move on to our specific field of interest/application.

1.2.1 Structural Health Monitoring (SHM) in large structures.

Structural Health Monitoring (SHM) refers to using sensor arrays to detect damage in engineering structures such as bridges or airplanes. SHM involves monitoring the dynamic responses from sensor arrays along the structure, especially the parts which are damage-sensitive, and use statistical analysis to determine a "state of health" for the structure. FO sensors has been gaining

significant attention in SHM over its electrical counterparts such as strain gauge or piezoelectric sensors, mainly due to its high sensitivity, multiplexing capabilities reduced requirement of wiring, and operability in a wide range of pressure environments [7].

Load monitoring, one of the critical aspects of SHM currently requires electrical strain gauges placed at limited number of points , typically 5 to 20 [7] each individually requiring dedicated electrical wiring leading to increased system complexity and cost. Fiber optic strain sensors are beginning to fill this gap with its multiplexing feature where multiple sensing points can be integrated into a single fiber and the signal can be read remotely with minimal electrical and thermal noise from the environment.

1.2.2 Biomedical Applications

With excellent sensing capabilities under electrical insulation and/or under electromagnetic interference environments, such as under Magnetic Resonance Imaging (MRI) or Radio Frequency (RF) treatments, fiber optic (FO) sensors have recently gained accelerated research attention in biomedical sensing applications. The physical parameters of interest in biomedical sensing, which could be measured using existing fiber optic sensors could be broadly classified into vital sign (temperature/heart rate etc.) and biochemical sensors. The latter will not be discussed here as it is out of scope of this research area.

During the years 2010-15, there have been extensive research focus on developing vital sign (temperature, breathing, heart rate etc.) monitoring systems using FO sensors [8]–[10]. In 2017, Fajkus et al [11] proposed a hybrid multichannel vital sign monitoring system using FBG sensors whose most important feature was that it could simultaneously process vital sign signals from 128 patients in a hospital setting even in a magnetic resonance environment. In addition to vital sign monitoring, FO sensors have found applications in another important field, i.e. thermal treatments in tumor removal. Thermal treatments such as RF/laser/microwave ablation involves inducing temperature changes locally in the tumor areas while leaving the healthy tissues undamaged. Monitoring the internal tissue temperature accurately and in a minimally invasive way was a critical need [12]. FO sensors, with its flexibility and sensitivity, turned out to be an excellent candidate to fill this gap. Schena et al recently (2016) reviewed the state of the art in FO sensing particularly in thermal treatments of tumors in [12]. Dziuda reviews applicable technologies in FO based vital signs monitoring especially during MRI procedures [13].

2 Classifying Fiber Optic Sensors

FO sensors can be largely classified into two major categories. **Extrinsic** FO sensors, where the actual sensing takes place outside the fiber, and the fiber is only used to guide the input light into the sensing region and back, are out of scope here. Only **Intrinsic** FO sensors, where the sensing takes place within the fiber are discussed here. Guo et al. in [7] , and Eric et al. in [4] have classified FO sensors into three general categories based on their operating principles: Interferometric sensors, distributed sensors and grating based sensors. Grating based sensors e.g. FBGs would be the focus of this thesis, the other two would be briefly described as background information.

2.1 Grating based sensors

The most commonly used grating based sensor is the Fiber Bragg Grating (FBG) sensor, where the refractive index of a portion of the core is manufactured to be periodically altered, creating a grating/reflector where only a certain wavelength is reflected satisfying the Bragg condition enabled by constructive interference (called the Bragg wavelength) while the rest is transmitted creating something like a stop-band optical filter. The grating pitch being sensitive to temperature and strain, shift in Bragg wavelength gives us information about the surrounding conditions, thus works as a sensor. Figure 1 illustrates the basic principle of operation for FBG sensors.

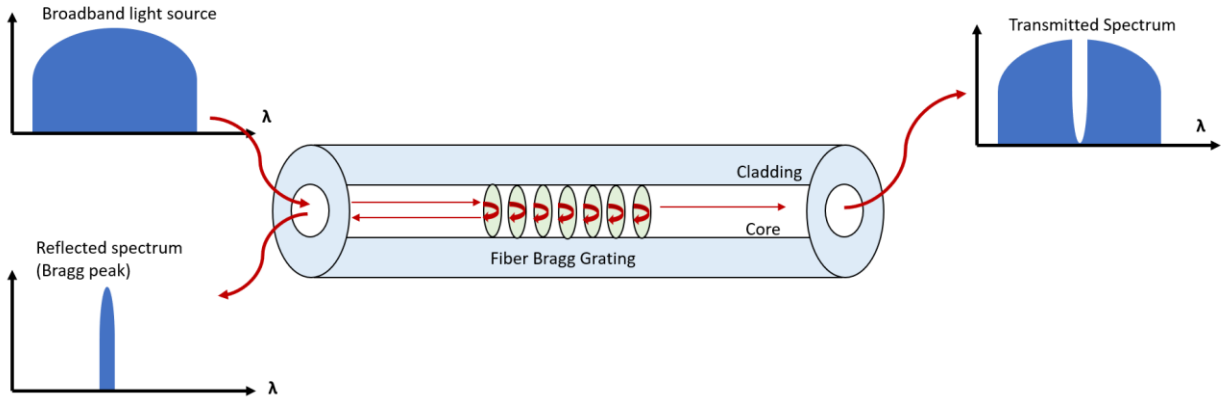

Figure 1 Illustrating Fiber Bragg Grating operating principle

Modern FBG fabrication techniques are broadly classified into two categories. First is the holographic method where a beam splitter is used to cause interference between a divided

ultraviolet (UV) beam. The second uses a masking technique to create the spatially periodic changes in refractive index (RI) along the fiber core. [14]

FBG sensors are widely used for temperature and strain/pressure sensing in structures. The major advantage of FBG sensors includes its ability of distributed sensing and multiplexing [4] which enables FBG sensors to be used for simultaneous measurement of temperature and strain in systems where accurate monitoring is required over the lifespan of the system. They also eliminate the need of two electrical leads in every measurement point as posed by electrical strain gauges [4] and enable multi-point measurement along the same fiber. FBG sensors are widely being used to sense strain, temperature, vibration etc. Successful research and experiments on simultaneous measurement of temperature and strain is already established in literature, e.g. using long period gratings [15], double cladding [16], hence are out of scope of this work.

2.2 Distributed FO Sensors

Distributed FO sensors, in general, exploit the scattering processes such as Raman, Brillouin, and Rayleigh scattering [4] occurring along the fiber. An optical signal is sent along the fiber and the backscattered signal is measured owing to its strong sensitivity to external conditions. What makes distributed FO sensors interesting is that it allows us to measure continuously along the length of the fiber without deploying specific sensing points. While Raman and Brillouin scattering has similar set up to measure temperature and strain, Rayleigh based FO sensing is a bit less straightforward, and typically used to measure “environment dependent propagation effects e.g. attenuation/gain” [17]. In general, distributed fiber optic sensors are used in cases where monitoring along a significantly long length or depth is required, e.g. oil pipes. Distributed sensors are out of the scope of this report.

2.3 Interferometric FO Sensors

Interferometric FO sensors are the largest subclass among all FO sensors [4]. Interferometric FO sensors use the interference between two beams with a path difference, one of them exposed to external measurands, and the received beam is analyzed to sense the external conditions. One of the reasons why interferometric FO sensors has received a lot of attention, is its ability to quantitatively analyze a number of wavelengths, phase, intensity etc. leading to an accurate measurement over a large dynamic range. They can also be miniaturized for micro-scale

applications [18]. Interferometric FO sensors go beyond temperature and strain sensing; many of the sensors which have already been developed or are being developed in various research labs, can also sense acceleration, acoustic waves, magnetic field, current, electric field, refractive index etc. generating an interest in a wide range of fields in science and technology.

An FO interferometer typically contains a beam splitting and a beam combining mechanism implemented in various ways depending on their type, to enable the interference process take place. The output optical signal is analyzed externally after exiting the combiner.

There are four major types of FO interferometers: Mach-Zehnder, Fabry-Perot, Sagnac and Michelson. Other types include Mode coupling, Ring resonator, and Polarization sensors as to be found in [4]. Due to the limited scope of this study, we will not discuss them further in this thesis.

3 Problem Area

Fiber optic (FO) sensors have been extensively studied for structural health monitoring and biomedical measurements in the past decade [7] by developing novel strain sensors. However, biomechanics, a field being a quantitative discipline largely depending on force/pressure measurements, is still not in full touch with the state of the art in FO sensor technologies. The majority of sensors being used in biomechanics research are still electrical/electronic biomechanical sensors, such as piezoelectric sensors. [19]. Biomechanics is defined as the mechanics of living bodies, in particular human bodies [19]. One of the broad classes of this field being the biomechanics of rigid (non-deformable) bodies, requires measurement of force under variable conditions to understand the dynamics of human bodies under impact or injury, or even for athletic workout. Little research has been done on developing or optimizing fiber optic sensors for biomechanical / bio- kinematic applications, although a bright future is envisioned by researchers in related areas.

In biomechanics, force platforms are the most common tool used in a lab. They are used in measuring the ground reaction force (or weight force) generated by a steady or moving (human) body to analyze biomechanical parameters such as balance and/or gait (movement pattern) [20]. Existing force plates either use piezoelectric sensors or strain gauges [19]. Data from the force plates are therefore often used in synchronization with other measurements such as limb kinematics (movement of points in the body) to get accurate analysis.

Force platforms are usually expensive, not portable, and difficult to operate. Typical price of a commercial force platform ranges from USD 10,000 to 20,000 [21]. The high costs associated with these platforms originate from sophisticated and complex mechanical structures and materials, electrical sensor assembly, and signal processing units. FBG sensors can potentially reduce these costs significantly [22].

A literature survey until August 2018 regarding a fiber optic force platform, verified by a review article on this field by Roriz et al [19], indicated that there are no fiber optic sensor based force platforms available neither in the market, nor has any been developed in any research group. However, it is widely agreed that the excellent multiplexing and distributive capabilities of fiber optic sensors, coupled with the strong sensitivity to strain, make fiber optic sensors potentially a very good candidate for force platform sensing in biomechanics. FO sensor array based force platforms may very well lead to the next generation high resolution force mapping. Research results using force platforms have always had a direct impact on the sports industry, for example, the development of athletic footwear.

4 Previous Works

Within the Photonics Applications Laboratory at Dalhousie University, a number of research works were done in the area of fiber optic sensors. Ma et al [23] developed a highly sensitive z-shaped interferometric sensor for refractive index sensing. Hochreiner et al [24], [25] worked on modeling and tuning long period fiber gratings for chemical sensing applications. Li Long [26] in his masters thesis (2010) designed and simulated a multi-axis FBG accelerometer. With a growing research attention to low-cost biomechanical force sensing area, this thesis explores the possibility of using the strain sensing capabilities of FBGs to measure higher ranges of biomechanical forces.

The state-of-the-art in FBG based sensors in biomechanical force sensing applications within the broader context of fiber optic sensors can be illustrated using the following diagram in Figure 2.

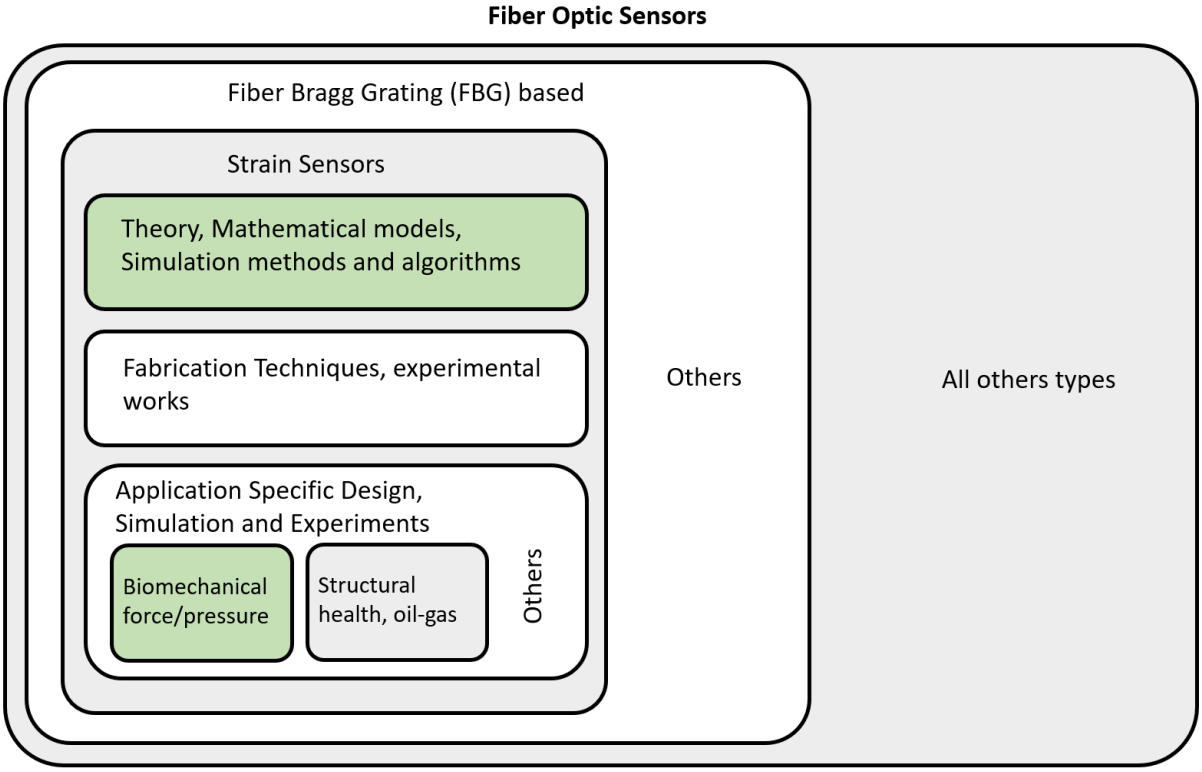

Figure 2 Visually illustrating the previous works in FBG sensors for biomechanics applications

Discussion in this section will be limited to FBG based sensors which are theoretically based on strain sensing, and works relevant to biomechanical pressure/force sensing only. There are other kinds of FO sensors than FBGs, and within FBGs, the literature is parted into sensing quantities other than strain e.g. temperature, humidity etc. Within the subclass FBG based strain sensors, the literature covers theoretical studies, mathematical models, simulation methods and experimental studies. FBG fabrication techniques are out of scope of this work, hence will not be discussed. The most recent research frontier in this subclass is application specific design, simulation and implementation/experiments. While the theoretical models for FBGs have matured, there is need to design specific use-cases/applications to implement sensing capabilities in reality. Since various applications demand specific designs, parameters and feasibility analysis, this area has been growing recently and new applications are being uncovered. The work in this thesis falls into this category where we would use the existing theoretical models and methods from the literature, and simulate the feasibility/behavior of using FBGs in a particular application: biomechanical force sensing. With relevance to the scope of this thesis, in this section, only the state of the art in the

theory, mathematical models, and simulation methods of FBG strain sensing, and the application specific design, simulation and experiments in biomechanical force/pressure sensing (shaded green in Figure 2) are discussed. Table 4-1 summarizes the theoretical foundations and the state-of-the-art in FBG based force sensing.

Table 4-1 Theoretical foundations and state-of-the-art summary of FBG based force sensing in biomechanics, theory, simulation, applications

Category	***State of the Art***	***References***
Theory	▪ The fundamental matrix approach for slab waveguides by Yamada and Sakuda (1987);	[27],
	▪ Modified T-Matrix method for FBGs by Peters et al. (1999-2000)	[28]
Simulation	▪ Characterizing Dynamic Strain measurement (2006)	[29]
	▪ Mid infrared FBG (numerical model, 2013)	[30]
	▪ FBG spectrum simulation tool by Pereira et al (2017), Correlating FBG simulation with FEM models, empirical validation	[31], [32]
	▪ Numerical simulation to detect damage in composite structures using FBGs; integrated FEM model of composite (Hassoon et al, 2015). Modeling and simulation for Oil/Gas sensing, biomedical applications	[33], [34]
Experiment	▪ Low temperature strain dependence (2006)	[35]
	▪ Reusable surface mounted FBG sensor (2016)	[36]
	▪ Force sensing using FBG (upto 60N)	[37]
	▪ Force Sensing using Birefringence (5kg resolution)	[38]
	▪ Foot pressure monitoring transducer for diabetic patients (lower range of force)	[39]
	▪ In-shoe monitoring of Ground Reaction Force (2018)	[40]
Applications	▪ Biomedical and Biomechanical pressure sensors	[41]

	▪ FO sensors in biomechanics (2018) ▪ FBG strain sensors, technology and applications review	[42] [19] [43]

The core theory of simulating the reflected spectra from an FBG stems from the theoretical works of Yamada and Sakuda (1987) for slab waveguides which introduced the fundamental matrix approach [27]. It was later modified by Peters et al [28] to work with more practical non-uniform strain fields and FBGs instead of slab waveguides. This work lays the foundation for the work of Pereira et al (2016-17) [31], [32] in developing an advanced computational algorithm to simulate FBG spectra which is also capable of extracting relevant stress-strain information from an FEM model to simulate the spectrum shift. While there are a few other works [33], [44] adopting similar approach to simulate FBG spectra based on FEM results, Pereira's work was found to be sufficiently comprehensive and repeatable to adapt in solving our problem. Also, the experimental verifications of their work were conclusive. While there have been some experimental works recently in developing force sensors using FO sensors, they have a common limitation of working in lower ranges of forces, suitable for various other low-range (~50N) applications. Extensive reviews by Roriz et al [19], [22], [42] point out the existence of a research gap in developing FO sensors for larger range (>1000N) force sensing applications such as in biomechanics force platforms.

5 Research Gap

FBGs are not directly sensitive to force, but longitudinal strain. Most studies have mainly focused on measuring strain using FBGs. However, studies on measuring transverse force, except very low ranges of force using the birefringence property [38], is very limited. Because of the low measurement ranges of force using birefringence, we need transducers for measuring higher ranges of force, i.e. something that translates high value of vertical forces into lower range of longitudinal strains in an operating range to not break the fiber. Transverse forces can induce strain via a transducer but it would also induce birefringence (peak splitting) limiting the quality of measuring the wavelength shifts. This causes practical limits on measurement precision.

The major practical challenges limiting the design of a transducer for this purpose are as follows:

- **FBG/Optical Fiber strain tolerance:** FBGs can at best tolerate 1% (10^4 $\mu\varepsilon$) strain [45].
- **Optical Spectrum Analyzer resolution:** The wavelength shifts resulting from the vertical forces in the operating range for this application must be such that they are well-detectable using typical lower cost spectrum analyzers. Typical resolution of this is 10 pm [14].
- **Transducer deformation:** A transducer in this scenario would convert vertical force into longitudinal strain via deforming the mechanical structure. Keeping the deformation minimum would be an important criterion.

In addition to these limitations, a gap still prevails in the literature on the evolution of spectral response quality in terms of FBG manufacturing parameters such as the FBG length and RI modulation depth. FBG length corresponds directly to the size of the sensor; therefore, analyzing the behavior or the spectral response quality in terms of FBG length will give us a solid idea about how small we can go for FBG sensors for this application. Note that the smaller the better for a dense array of FBG sensors. Moreover, with new advanced technologies in FBG fabrication, modulation depth can be precisely controlled. As it is derived from the theory, it highly affects the reflected spectrum in terms of reflectivity and bandwidth. However, a systematic analysis of FBG spectrum evolution with respect to modulation depth for such an application is not found in literature. To be able to properly design a working transducer, it is required to find out what FBG fabrication parameters should we choose and why, and only then it is possible to move into designing a system that meets the required criteria.

6 Contribution

In this thesis, it is quantitatively proved that it is feasible to develop a lightweight, low-cost, EMI immune, electrically isolated force platform based on FBGs for biomechanics applications despite its limitations. While the theory of FBGs are known, and simulation methods are available, this application is pointed out in the literature to be necessary, yet no work has been done so far in this area.

The contribution of this thesis is mainly twofold:

First: the quality of the reflected spectra from an FBG was systematically analyzed with respect to two FBG fabrication parameters, FBG length and modulation depth. Optimum ranges of these for a biomechanical force sensing application were determined.

Second: a simplified finite element model of a force platform is developed, and a static analysis is performed to estimate its behavior under realistic ranges of forces for biomechanics applications. Information from the model were used to simulate the characteristic of the reflected spectra using established theoretical models from the FBG literature. Necessary fabrication parameters were derived from the previous step. The major contributor of signal distortion would be transverse force causing birefringence (peak splitting). This would also be analyzed while presenting the results.

The contributions of this thesis are submitted for publication in the Sensors Journal [46].

7 Method

The simulation method can be broadly divided into two parts: First, simulating the FBG reflected spectra for different FBG parameters, e.g. length and modulation depth. That would give us optimum parameters for use with this application. Second: a finite element method simulation of a mechanical transducer that would convert vertical force into longitudinal strain on the fiber, which would result measurable spectrum shift in the FBG reflected spectra. Results from the FEM simulation would lead us to approximate this spectrum shift.

Simulating the FBG reflected spectra for different FBG parameters: A Python based simulator developed by Pereira et. al [31] based on established theories from the literature, e.g. the basic FBG equations, the coupled mode theory, and the transfer matrix method will be used to simulate the evolution of the FBG reflected spectra with respect to varying FBG length and modulation depth under no-load conditions. From this, optimum ranges of these parameters will be derived for the intended application of this work. The main reason for choosing the T-matrix method over the beam propagation method [47] is that in beam propagation method, the effect of the reflected field on the forward propagating field is not considered. In FBG based strain sensing, the interaction between the forward and backward propagating modes is crucial to determine the nature of the reflected spectra that is measured to calculate strain. That is why the beam

propagation method is mostly used to model long period gratings where only coupling between forward propagating modes are of interest.

Finite element method simulation of a mechanical transducer: A finite element model of a mechanical transducer that would convert vertical applied force into strain along the fiber will be developed using the commercial FEA tool Abaqus CAE. Abaqus is a powerful and widely used software suite for Finite Element Analysis and Computer Aided Engineering (CAE). It is mostly used in mechanical and civil engineering disciplines to model complex structures and simulate their mechanical behaviors. Within the scope of this work, this tool fits the need to analyze the mechanical transducer, i.e. the force platform given that we would define the physical structure, know the mechanical properties of the materials used, and the loading ranges corresponding to this application, and the stresses and strain at every location (element) of the transducer are to be calculated. This information would be processed using Pereira's simulator to construct the spectrum shift due to strain, and the polarization split due to the birefringence effect caused by transverse stresses. The link between the FEM model and the FBG will be established by the simulator by matching the number of elements containing the FBG and the number of small T-matrix segments that the algorithm uses to divide the total FBG length. Further details are explained in Chapter 2, Section 9.3. An illustration of the method is shown in Figure 3.

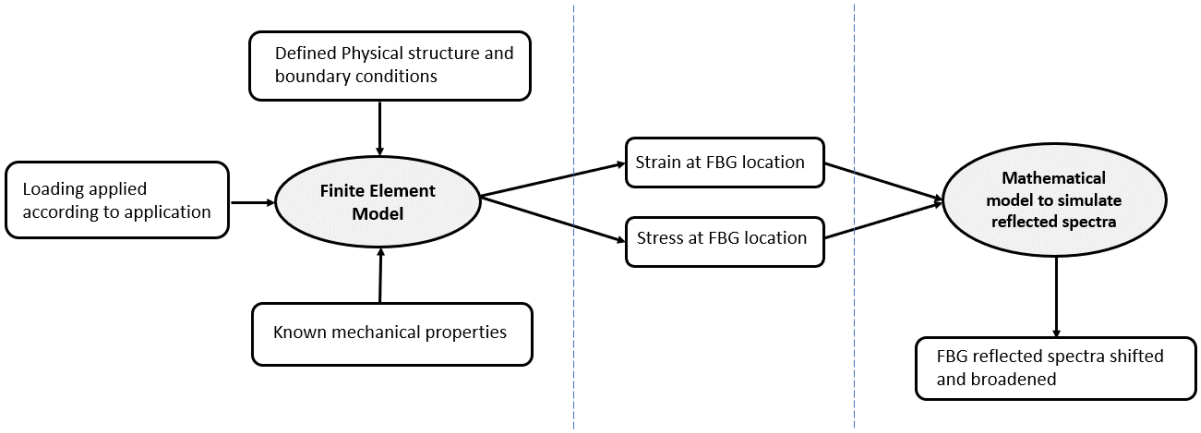

Figure 3 Illustrating the method adopted in this thesis

8 Organization of the Thesis

Chapter 2 describes the theoretical foundations of the work. In dedicated sections it describes the basic FBG relationships, the coupled mode theory, and the T-matrix method and how they all come together to enable an FBG spectrum simulation for specific applications. **Chapter 3** describes all the simulation results; first the FBG parametric simulation under no load, and second, the FBG reflected spectrum after connecting it to the results of the FEM model. **Chapter 4** wraps up the discussion with concluding remarks and future works.

Chapter 2
Theory and Simulation Model

Three sets of theoretical background are necessary to understand the FBG spectrum simulation. Starting with the basic FBG relationships, in this chapter, it is shown how the coupled mode theory (CMT) and the Transfer Matrix Method are used together to simulate the FBG spectra. In addition, the effect of birefringence on the FBG reflected spectra in this application is described with necessary background explanation.

9 Theory

9.1 Basic FBG Relationships

When there is no external strain acting on the FBG and the temperature is constant, the position of the peak at the reflected spectrum of a homogeneous FBG is given by the following relationship, also known as the Bragg condition, in (1):

$$\lambda_B = 2n_{eff}\Lambda_0 \tag{1}$$

Where:

λ_B = Reflected Bragg Wavelength

n_{eff} = Effective Refractive Index (RI) at the grating

Λ_0= Grating pitch, or the period of RI modulation

It is be observed that the position of the reflected Bragg wavelength peak position depends on two parameters, the effective RI and the grating pitch.

An applied strain on an FBG induces two changes, the grating period, and the mean RI. If the strain field is assumed to be piecewise continuous, these two effects can be linearly superimposed, and we can simplify the expression of the grating period by introducing an effective strain $+(1-p_e)\varepsilon(x)$ to the grating [32], [48]. The change in the grating period can be expressed as a function of distance *(x)* along the fiber according to the following relationship: [31], [32], [48]

$$\Lambda(x) = \Lambda_0[1 + (1 - p_e)\varepsilon(x)] \quad (2)$$

Where:

p_e = Photo-elastic coefficient

$\varepsilon(x)$ = Strain variation along x

Λ_0= Grating pitch, or the period of RI modulation

p_e can be defined as: $p_e = \frac{{n_{eff}}^2}{2}[p_{12} - \nu(p_{11} + p_{12})]$

Where p_{11} and p_{12} are components from the fiber optic strain tensor, or Pockel's constants of the fiber. These are fiber dependent quantities and their values are determined experimentally [49]. For bulk silica, the values were found to be $p_{11} = 0.121$ and $p_{12} = 0.270$ [49]. ν is the Poisson Ratio of the fiber.

The other parameter that drives the Bragg wavelength shift is the effective refractive index (RI) change $\delta_{n_{eff}}(x)$, which varies spatially as a function of distance, and depends on the grating chirp $\phi(x)$ [34], [48]:

$$\delta_{n_{eff}}(x) = \overline{\delta_{n_{eff}}}\{1 + \nu\, cos[\frac{2\pi}{\Lambda_0}x + \phi(x)]\} \quad (3)$$

Where:

$\overline{\delta_{n_{eff}}}$ = dc effective refractive index (RI) change; modulation depth

ν = Fringe visibility $\approx$ 1

Λ_0= Grating pitch, or the period of RI modulation

For a uniform longitudinal strain applied on a FBG, the shift in Bragg wavelength can be simplified to the following relationship [34]

$$\Delta\lambda_{strain} = \lambda_B(1 - p_e)\varepsilon \quad (4)$$

Where $\Delta\lambda_{strain}$ is the Bragg wavelength shift from the original wavelength λ_B, due to strain ε along the fiber.

This shows that the position of the shifted Bragg wavelength largely depends on the applied strain and the strain optic properties of the fiber. However, to fully simulate the characteristics of an FBG reflected spectra, we need the amplitude/reflectivity of the FBG spectra along with how it will be distributed in the wavelength domain. For that, the Coupled Mode theory is utilized.

9.2 Determining the peak shape: Coupled Mode Theory (CMT)

To characterize the transmitted and reflected spectra in terms of reflectivity and the shape of the spectra, the most powerful mathematical tool is the Coupled Mode Theory (CMT) which gives us relationships between the forward and backward propagating modes along the grating. [31], [34], [48]

CMT gives us the following first order differential relationship describing counter propagating modes along the fiber direction. The Transfer Matrix method is used to solve these equations, as will be described in the next section.

$$\frac{d}{dx}R(x) = i\hat{\sigma}R(x) + i\,\kappa\,S(x) \tag{5}$$

$$\frac{d}{dx}S(x) = i\hat{\sigma}S(x) + i\,\kappa\,R(x) \tag{6}$$

Where:

$R(x)$ = Amplitude of the forward propagating mode

$S(x)$ = Amplitude of the backward propagating mode

$\hat{\sigma}$ = General DC self coupling coefficient; this is a function of the propagating wavelength, λ

κ= 'ac' coupling coefficient between counter propagating modes.

The coupling coefficients are defined as follows:

$$\hat{\sigma} = 2\pi n_{eff}\left(\frac{1}{\lambda} - \frac{1}{\lambda_B}\right) + \frac{2\pi}{\lambda}\overline{\delta_{n_{eff}}} - \frac{1}{2}\phi'(x) \tag{7}$$

$$= 2\pi n_{eff}\left(\frac{1}{\lambda} - \frac{1}{\lambda_B}\right) + \frac{2\pi}{\lambda}\overline{\delta_{n_{eff}}}$$

$$[\ \phi'(x) = 0 \text{ for uniform grating}]$$

$$\kappa = \frac{\pi}{\lambda} m \overline{\delta_{n_{eff}}} \tag{8}$$

Where m = Striate visibility $\approx$ 1

9.3 The Transfer Matrix (T- Matrix) Method and Connecting with Finite Element Model (FEM)

Yamada et al. [27] developed the Transfer Matrix method to simulate the characteristics of the reflected spectra from gratings in a slab waveguide. The key in this approach was to consider the waveguide as a series of short segments where gratings could be assumed periodic. This ensured that within each short segment, parameters such as coupling coefficient do not depend on the direction of propagation. The final output of the grating was obtained by multiplying the matrices corresponding to each segment and obtaining a final transfer matrix describing the overall grating.

Although this method was built for uniform strain fields, it was later modified by Peters et al. [48] and others [29], [30], [50] for non-uniform strain fields and in particular to Fiber Bragg Gratings (FBG). Peters et al. divided the fiber grating into smaller pieces of periodic gratings and calculated the responses of each segment by Yamada's method.

From Peters et al.'s work, when a strain is applied, the deformed grating period is calculated using the strain values in that particular segment. The final output is constructed using the combination of all segments in the T-matrix method. This is important because it lays the foundation of using Finite Element Method (FEM) Models to simulate the FBG reflected spectra using stress-strain information extracted from the FEM.

In an FEM model of a structure, the structure is divided into many small “elements”. Each element in a mechanical FEM model contains information about stress and strain in that element, which in turn, combining with all other elements, describe the behavior of the entire structure.

In T-matrix method, the grating is divided into short segments, and the resultant spectra is formed due to the contribution from each segment. In FEM models, the structure is divided into many small elements. Pereira [31], [32] and others [33], [44] successfully demonstrated that it is possible to simulate FBG spectra using information from an FEM model if the number of short segments in the T-matrix method and the number of elements in the FEM model are matched. A Python based simulator developed by Pereira [31] will be used in this work. Figure 4 illustrates the T-matrix method for simulating FBG spectra with finite sectioning and exemplifies its connection to structural FEM models by element-matching.

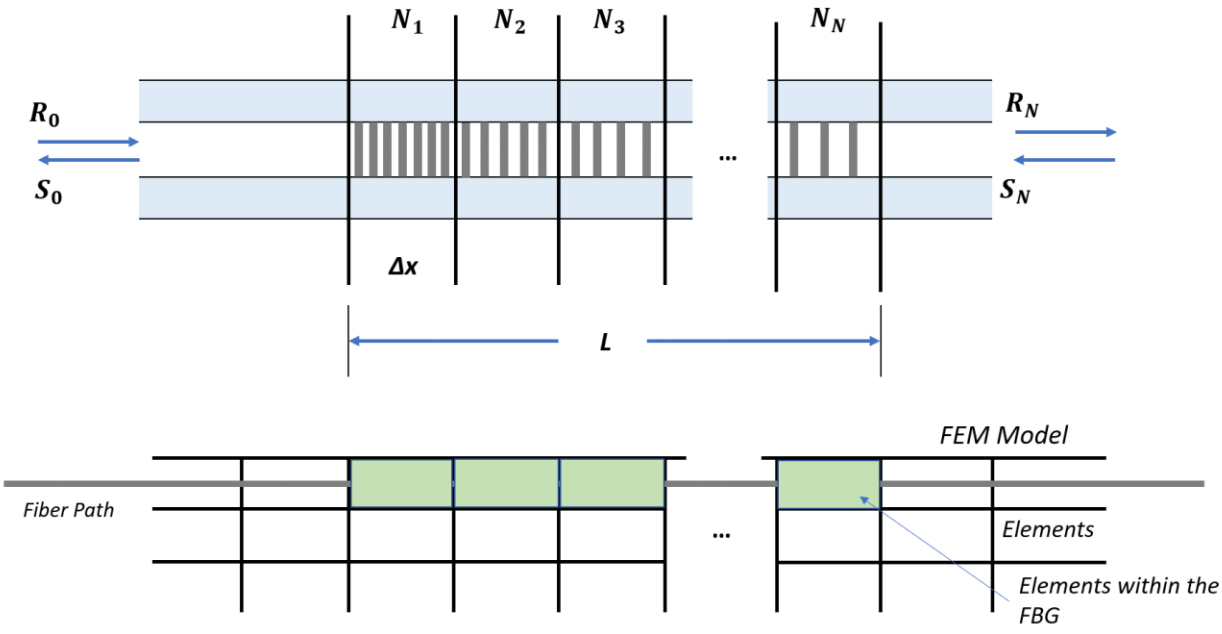

Figure 4 Illustration of T-Matrix method and connecting it with FEM model

The T-matrix method helps us solve the Coupled Mode equations of the grating and hence reconstruct the FBG spectra.

Let the grating length be *L*. This is divided into *N* segments. Each segment is $\Delta x = L/N$ long.

The accuracy of the model should depend on a larger value of *N*, However, *N* cannot be arbitrarily large, as we must have sufficient periods in each segment to complete the coupling [29]. The constrain for *N* is derived in [29] as:

$$N \leq \frac{2n_{eff}L}{\lambda_B} \tag{9}$$

Where:

L = grating length

λ_B= Original Bragg Wavelength

The grating length *L* sets the limit of *x* as follows:

$$-\frac{L}{2} \leq x \leq \frac{L}{2}$$

The boundary conditions on forward/backward propagating modes are:

$$R\left(-\frac{L}{2}\right) = 1$$

$$S(\frac{L}{2}) = 0$$

The reflectivity is [29], [31]:

$$r(\lambda) = \left|\frac{S(-\frac{L}{2})}{R(-\frac{L}{2})}\right|^2 \tag{10}$$

To find out the right hand side quantities, we need to employ the T-matrix solutions.

If the subscripts (*i, i-1*) denote the forward (R) and backward (S) propagating modes' amplitudes after and before the i^{th} segment in grating, the following can be written in matrix form [29], [31], [34]:

$$\begin{bmatrix} R_i \\ S_i \end{bmatrix} = F_i \begin{bmatrix} R_{i-1} \\ S_{i-1} \end{bmatrix} = \begin{bmatrix} F_{11} & F_{12} \\ F_{21} & F_{22} \end{bmatrix} \begin{bmatrix} R_{i-1} \\ S_{i-1} \end{bmatrix} \tag{11}$$

The transfer matrix components are described as:

$$F_{11} = {F_{22}}^* = cosh(\gamma_B \Delta x) - i\frac{\hat{\sigma}}{\gamma_B} sinh(\gamma_B \Delta x)$$

$$F_{12} = {F_{21}}^* = -i\frac{\kappa}{\gamma_B} sinh(\gamma_B \Delta x)$$

Where:

$$\Delta x = \text{length of the section}$$

$$\gamma_B = \sqrt{\kappa^2 - \hat{\sigma}^2}$$

Finally, the total grating transfer matrix would be:

$$F = F_1 . F_2 . F_3 \ldots F_N \tag{12}$$

Therefore:

$$\begin{bmatrix} R_N \\ S_N \end{bmatrix} = F \begin{bmatrix} R_0 \\ S_0 \end{bmatrix} \tag{13}$$

Hence, the reflectivity equation [29], [31], [34]:

$$r(\lambda) = \left|\frac{S\left(-\frac{L}{2}\right)}{R\left(-\frac{L}{2}\right)}\right|^2 = \left|\frac{F_{21}}{F_{11}}\right|^2 \tag{14}$$

9.4 Effect of Birefringence on FBG (Peak splitting)

When measurement of force is the primary function of the FBG sensor, stress induced birefringence is a key source of distortion in FBG reflected spectra by means of peak splitting [51].

When an FBG is subject to transverse force in the z-direction, as shown in Figure 5, two different stresses (σ_z, σ_y) are generated in the Z and Y directions respectively. This changes the refractive indices in these two directions, resulting in creating two orthogonal polarization modes that are perceived as the original FBG peak being split into two (Figure 6). The change in the effective refractive indices in these orthogonal polarization states, Δn_z and Δn_y are described as in equations (15) and (16):

$$\Delta n_z = -\frac{{n_0}^3}{2E_F}\{(p_{11} - 2\nu_F p_{12})\sigma_z + [(1-\nu_F)p_{12} - \nu_F p_{11}](\sigma_x + \sigma_y)\} \tag{15}$$

$$\Delta n_y = -\frac{{n_0}^3}{2E_F}\{(p_{11} - 2\nu_F p_{12})\sigma_y + [(1-\nu_F)p_{12} - \nu_F p_{11}](\sigma_x + \sigma_z)\} \tag{16}$$

Where:

E_F = Young modulus of the fiber

ν_F = Poisson ratio of the fiber

n_0 = Initial effective refractive index

$\sigma_z, \sigma_y, \sigma_z$ = stress components in the subscripted directions.

p_{11}, p_{12} = Pockel's coefficients

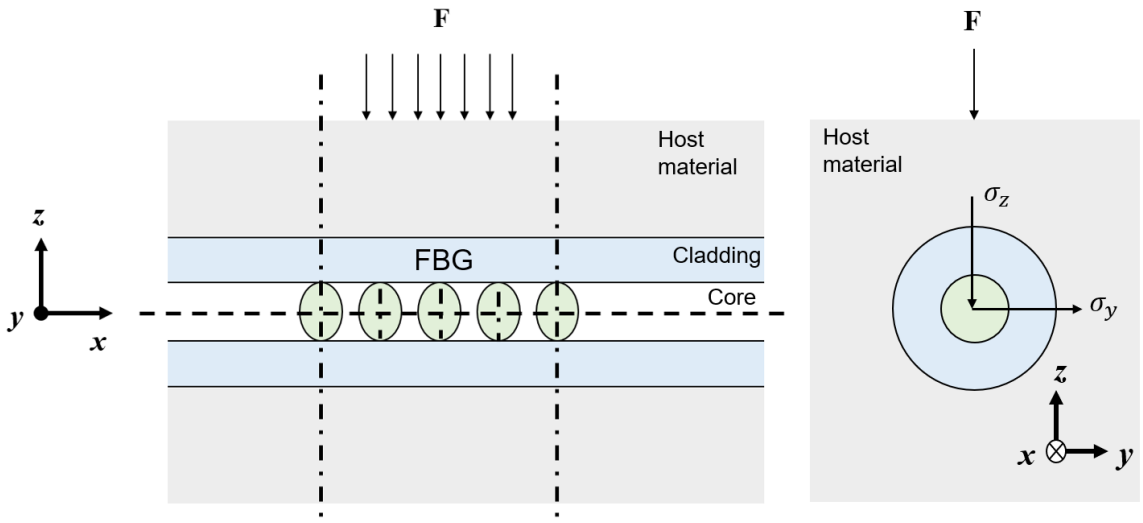

Figure 5: Fiber Bragg Grating (FBG) under transverse force

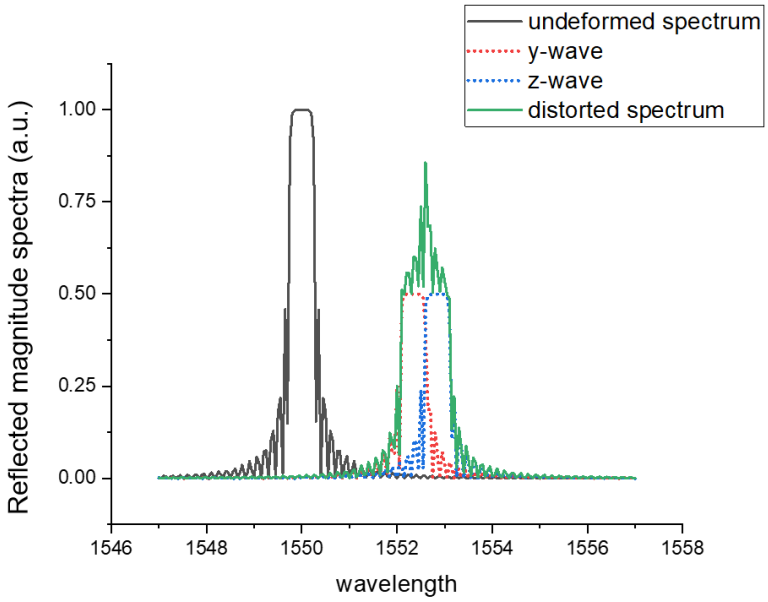

Figure 6 the effect of transverse force on the reflected spectra from the FBG due to stress induced birefringence

With this birefringence effect, the FBG reflects two peaks at λ_z and λ_y, corresponding to their polarization states as in Figure 6. In other words, transverse stress causes the Bragg reflected peak to split. From equations (1),(15) and (16), the spectral separation is found to be [32], [51] :

$$\begin{aligned}\Delta\lambda &= \left|\lambda_z - \lambda_y\right| \\ &= 2\Lambda\left|\Delta n_z - \Delta n_y\right| \\ &= \frac{\Lambda {n_0}^3}{E_F}[(1+\nu_F)p_{11} - (1-\nu_F)p_{12}].\left|\sigma_z - \sigma_y\right|\end{aligned} \tag{17}$$

10 Simulation Method and Tools Used

The FBG simulator developed by Pereira et al [31] based on the basic FBG equations, the Coupled Mode Theory and the Transfer Matrix Method was used to simulate the FBG reflected spectra for varying FBG fabrication parameters for unperturbed (no-load) condition. A range of these parameters most suitable for the intended application were derived, which was used to simulate the FBG reflected spectrum when loads are applied on the transducer that will be designed.

A physical design of a mechanical transducer capable of translating transverse force into longitudinal strain acting on a fiber was introduced. The amount of force applied to the transducer was known, but the amount of stress and strain that would actually be acting on the FBG was not known. To estimate the amount of stresses and strains acting on a possible FBG location during transverse loading, a finite element model of this structure will be developed using the commercial FEM tool Abaqus CAE. There are practical limitations of using optical fibers and FBGs with respect to their strain tolerance and other factors (more on this in Section 12.2), hence the design must pass a set of requirements, which will be taken into account.

Once the FEM model was developed, the simulator was be fed with the results of the FEM analysis (Abaqus) along the intended fiber path, and the expected FBG location will be specified. The simulator matched the number of T-matrix segments to the FEM elements that contain the FBG to solve the CMT equations and output the reflected spectrum data. First, the effect of birefringence will be ignored to find out the nature of spectrum shift without distortion. Secondly, the polarization modes will be extracted (due to stress in the FBG location) to estimate the peak-split.

A summary of the method is illustrated in Figure 7. Also, a summary of calculation steps is illustrated in Figure 8.

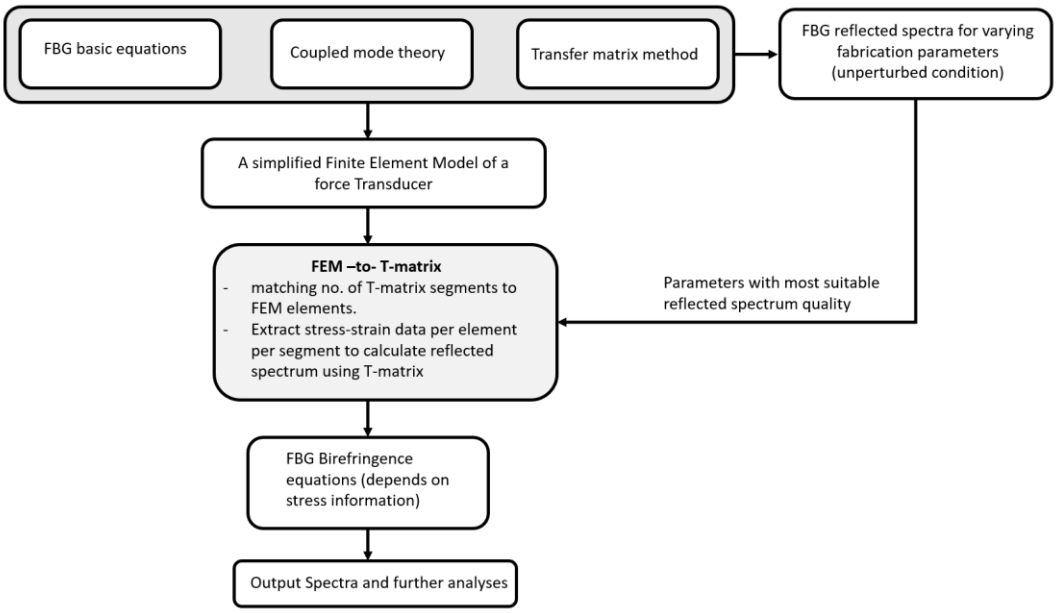

Figure 7 Summary of simulation method to be followed

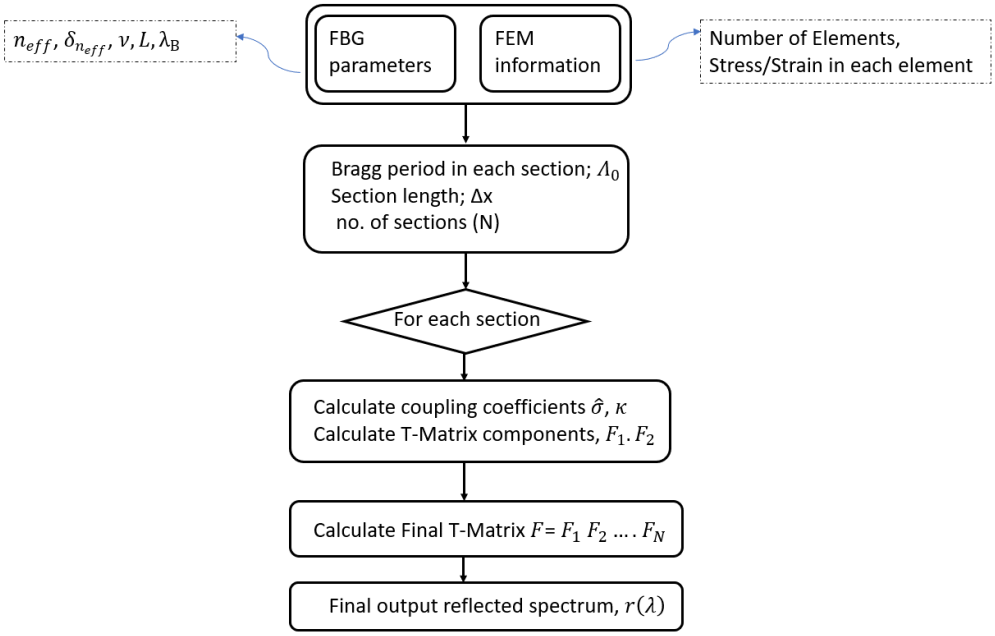

Figure 8 Summary of FBG spectrum simulation adapted from Pereira et. al [31]

Chapter 3
Simulation Results and Analysis

The simulations are performed in three stages:

The first step is a parametric simulation under no load. In this step, the force platform is not involved, only FBG length and modulation depth varied, one parameter at a time, while keeping others at their standard values. From this step we calculated an optimum range of FBG length and modulation depth that we can use in the next simulations involving the load and the transducer.

The second step is the physical design and FEM model of the transducer using Abaqus CAE. In this step we would apply a suitable range of force (from literature) for applications in biomechanical force sensing, such as in a force platform.

In the third step, the stress-strain static analysis results from the second step will be taken back to the FBG spectrum simulator and the nature of spectrum shift and birefringence distortion will be analyzed.

11 FBG Simulation Results (Parametric, No Load)

In this section, the effect of FBG Length (L) and modulation depth $\overline{\delta_{n_{eff}}}$ will be studied. It is important to study the effect of FBG Length (L) because this would give us a limit on how small we can go for the grating length, which would eventually determine how densely we can pack FBG arrays for this application.

The dc RI change ($\overline{\delta_{n_{eff}}}$) or modulation depth is important because the width of the reflected spectra from an FBG should depend on this parameter, which eventually determines how many wavelengths (sensors) can be multiplexed in an FBG sensor array for a force sensing application.

11.1 Parameters

Most parameters for FBGs are usually standardized based on the optical fiber material properties. Grating length and modulation depth are usually set while fabricating the gratings. Typical range of grating length in similar applications go from 1mm to 10mm, while modulation depth ranges from 1×10^{-4} to 10×10^{-4} . While studying the effect of FBG length, modulation depth will be

held fixed at 5×10^{-4}. While studying the effect of modulation depth, the FBG length will be held fixed at 5mm.

The fixed and variable parameters in this simulation are summarized in Table 11-1.

Table 11-1 FBG spectrum Simulation Parameters

Parameter name	Value
Grating length (L)	- varies from 1mm to 10mm while $\overline{\delta_{n_{eff}}} = 5 \times 10^{-4}$ - to study the effect of $\overline{\delta_{n_{eff}}}$, L is fixed at 5mm
"DC" refractive index change ($\overline{\delta_{n_{eff}}}$)	- varies from 1×10^{-4} to 10×10^{-4} when L= 5mm - to study FBG length L, $\overline{\delta_{n_{eff}}}$= 5×10^{-4}
Effective Refractive Index (RI) at the grating n_{eff}	1.46
Wavelength used	1550 nm
Photo-elastic coefficient, p_e	0.215
Fringe visibility	1
Pockel's constants of the fiber	$p_{11} = 0.121$; $p_{12} = 0.270$
Young modulus of fiber	$75 \times 10^9\ Pa$
Poisson ratio of the fiber	0.17

11.2 Quantities Analyzed

The quality of the reflected spectra from an FBG can be realized using the following three quantities:

1) **Reflectivity (R) of the grating**: higher reflectivity is desired for any application, maximum value is 1. It is understood from the theory that the FBG reflected spectrum would suffer from not only noise, but also birefringence effect. By ensuring the reflectivity to be maximum, it is possible to minimize the effect of these signal distortions.

2) **Full width at half maximum (FWHM)** of the reflected spectrum: We require narrow band peak for better detection of the signal and better multiplexing and utilization of the bandwidth of the input light. This is measured from the reflected spectrum of each simulation step.

3) **Sidelobe-level**: We also require better suppressed sidelobes while ensuring better reflectivity and narrow-band output. Therefore, absolute strength of sidelobe might be misleading, as in that case we can easily get suppressed sidelobes at lower reflectivity. To illustrate the effect of sidelobes as a performance indicator quantity, the ratio of the maximum sidelobe magnitude to the main lobe magnitude is expressed as side-lobe level or sidelobe-ratio.

11.3 Effect of Varying FBG Length (L)

Varying the FBG length from 1mm to 10mm with an interval of 1mm, the evolution of the reflected spectrum is illustrated in Figure 10 and Figure 11. More specifically, with respect to the quantities analyzed (Section 11.2), the evolution of reflectivity, side-lobe levels, and FWHM is summarized in Figure 9.

As we can observe in Figure 9, the reflectivity is too low (below 0.6) for FBG length =1mm. It changes rapidly from 1 to 2 mm and reaches 0.9. For 3mm length, it reaches very close to 1 and stays 1 from 4mm onwards. Higher FBG length clearly result in higher reflectivity. However, this characteristic tells us that for applications in force/impact sensing (e.g. biomechanics), we cannot consider a spatial resolution of FBG arrays closer than 2-3mm because of low reflectivity.

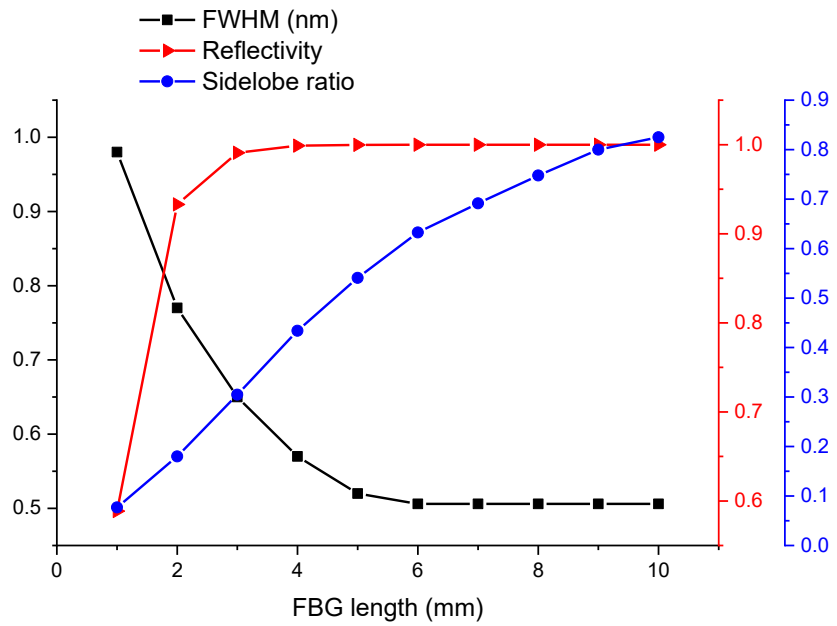

Figure 9 Reflectivity, FWHM and SLR change with varying FBG length

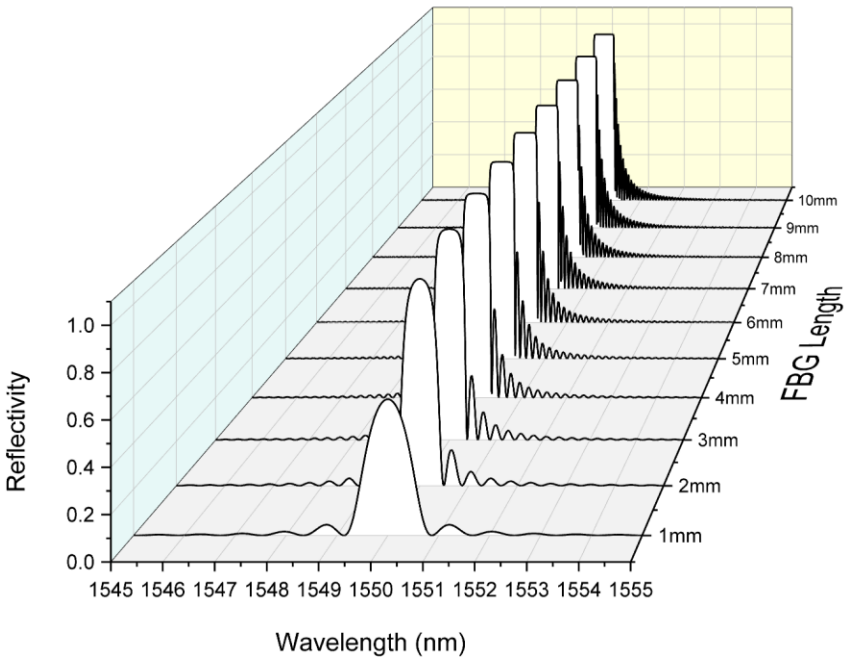

Figure 10 Evolution of FBG reflected spectra with increasing FBG length

We also observe that the FWHM reduces with increased FBG length. Higher FBG length means narrower reflected peak which is desirable. After L= 6mm, the FWHM settles to 0.5nm.

With other parameters held constant at the values fixed in this simulation, especially the modulation depth, the spectrum cannot be made any narrower.

The strength of the sidelobes increase with increased FBG length. This is also visible qualitatively from Figure 10 and Figure 11.

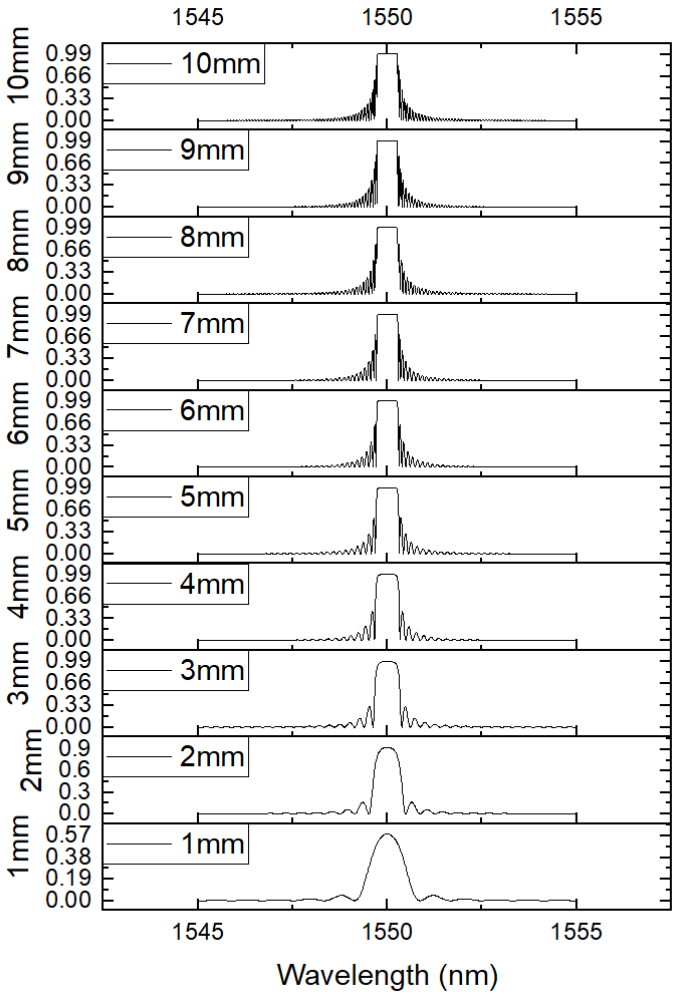

Figure 11 Evolution of FBG reflected spectra with increasing FBG length

These observations lead us to conclude that in the range of 3 to 5mm for the FBG length, we have a considerably narrow FWHM, a high reflectivity (0.9-1.0), and the first sidelobe not exceeding 60% of the main lobe magnitude. Therefore, this should be the range of FBG length we could be using for a force sensing application given the understanding that 3mm would be our limit in designing dense FBG sensor arrays.

11.4 Effect of Varying Modulation Depth ($\overline{\delta_{n_{eff}}}$)

Varying the modulation depth from ($\overline{\delta_{n_{eff}}}$) from 1×10^{-4} to 10×10^{-4}, with an interval of 1×10^{-4}, the evolution of the reflected spectrum is illustrated in Figure 13 and Figure 14. More

specifically, with respect to the quantities analyzed (Section 11.2), the evolution of reflectivity, side-lobe levels, and FWHM is summarized in Figure 12.

As we can observe from Figure 12, the reflectivity is too low (below 0.6) for $\overline{\delta_{n_{eff}}}$ =1 × 10^{-4}. It changes rapidly from 1 to 2 × 10^{-4} and reaches 0.9. For 3× 10^{-4}, it reaches very close to 1 and stays 1 onwards. Higher modulation depth clearly result in higher reflectivity. However, this characteristic tells us that for most applications, we cannot consider having RI modulation lower than 2-3× 10^{-4}.

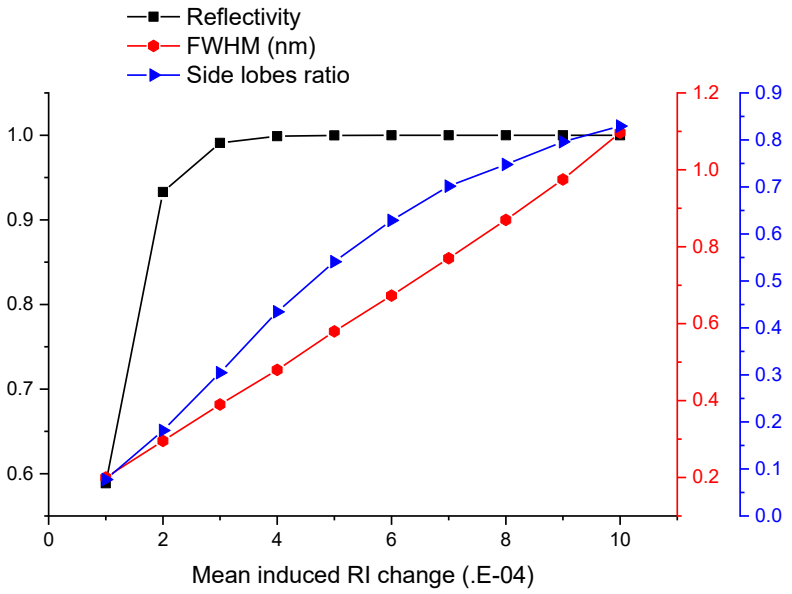

Figure 12 Reflectivity, FWHM and SLR change with varying dc RI change

However, we also observe that the FWHM increases with increased modulation depth. Higher modulation depth means broader reflected peak which is not desirable for proper wavelength selection and multiplexing. The FWHM does not settle down until the final value of dc RI change, rather it keeps increasing.

With other parameters held constant at the values fixed in this simulation, especially the FBG length, the spectrum cannot be made any narrower than FWHM=0.3nm without compromising

the reflectivity drastically. The strength of the sidelobes increase with increased $\overline{\delta_{n_{eff}}}$. This is also visible qualitatively from Figure 13 and Figure 14.

From $\overline{\delta_{n_{eff}}} = 3 - 5 \times 10^{-4}$, we have a considerably narrow FWHM, a high reflectivity (0.9-1.0), and the first sidelobe not exceeding 60% of the main lobe magnitude. Hence, this should be the range of modulation depth that we could be using for a force sensing application given the understanding that 0.6nm would be our expected FWHM to be detected by wavelength meter.

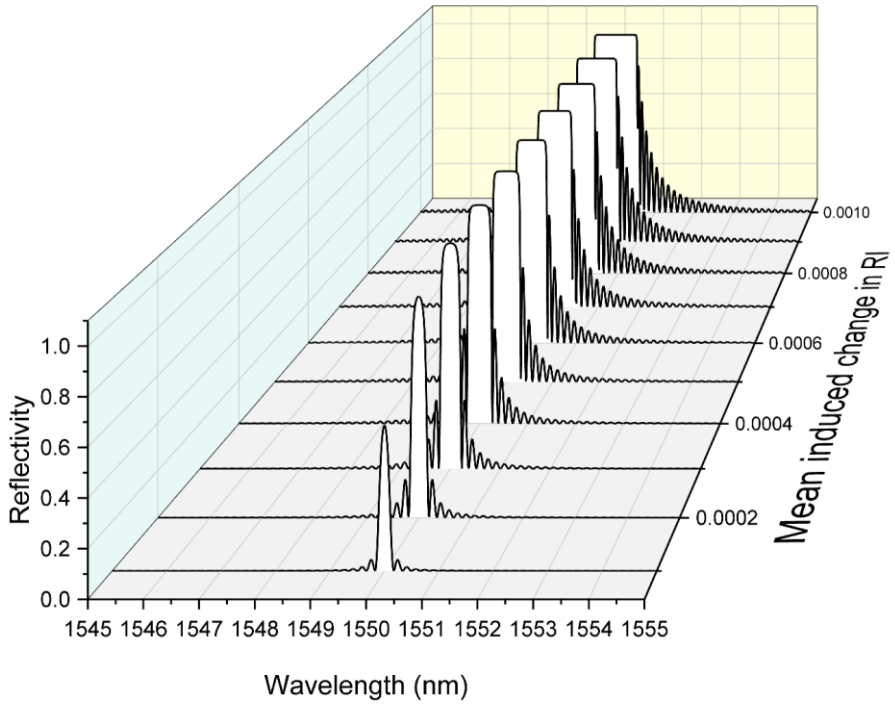

Figure 13 Evolution of FBG reflected spectra with increasing dc RI change

11.5 Summary of FBG Simulation Results

From the FBG parametric simulation, we found out that:

1) In the FBG length range 3-5mm, with modulation depth fixed at 5×10^{-4}, we get over 90% reflectivity with less than 60% sidelobe level and a low stabilized FWHM at 0.5nm.

2) In the modulation depth range of 3-5$\times 10^{-4}$, we get over we get over 90% reflectivity with less than 60% sidelobe level and a FWHM at 0.4-0.6nm.

In the next simulations, we will set L=5mm, and $\overline{\delta_{n_{eff}}} = 4.5 \times 10^{-4}$.

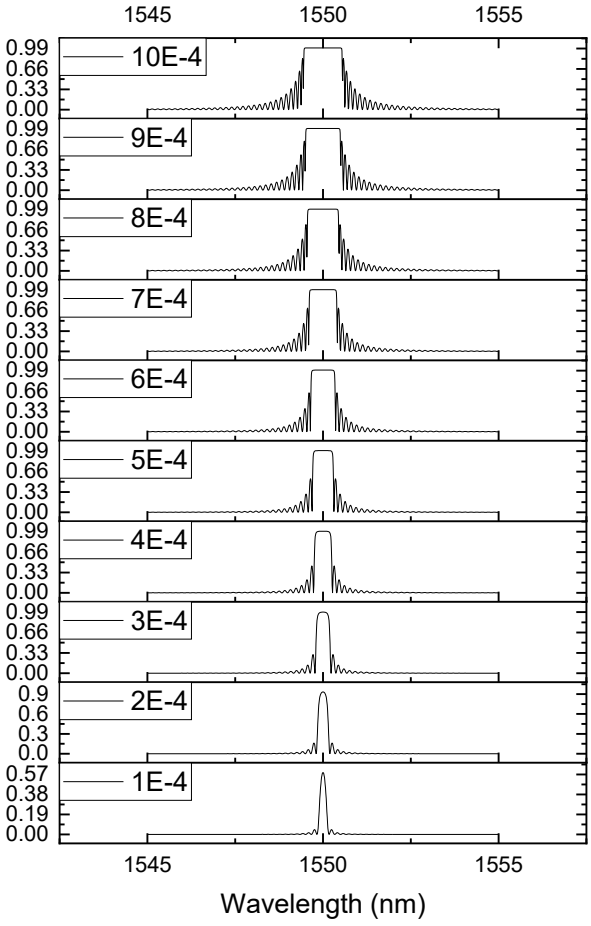

Figure 14 Evolution of FBG reflected spectra with increasing modulation depth

12 FEM Model of a Simplified Force Platform

12.1 Approach

Now that the FBG parameters are known, the next step is to design a transducer capable of delivering measurable spectrum shift from an FBG. To design a transducer, the requirements of this application are to be understood. FEM simulations were iterated in Abaqus to find a configuration that works with the requirements.

12.2 Requirements

The transducer must meet the following requirements:

- The design must be able to operate in the force range of 500N (body weight) to 7000N (peak landing force), which is typical for a biomechanical force sensing application, i.e. a force platform to measure standing and jumping force of an athlete. [19]

- The strain propagated to the fiber inside the structure as a result of the vertical force should be within typical fiber tolerance, which is 1% or 10^4 $\mu\epsilon$.[45] In other words, the propagated strain must not break the fiber.

- The strain acting on the FBG should also be large enough to generate a measurable spectrum shift. That means it must be detectable using standard spectrum analyzers. In other words, the spectrum shifts must be greater than a typical spectrum analyzer's resolution, which is 0.01nm [14].

- Transverse force distorts the reflected spectrum from the FBGs due to birefringence. So, the design should be such that the spectrum broadening/peak splitting due to transverse stress is significantly lower than the spectrum shift due to longitudinal strain.

- Structural deformation (especially vertical) of the platform should be minimized and kept reasonable.

12.3 Physical Design

12.3.1 The Force Platform

12.3.1.1 Geometry

For the force platform, we propose a 3 layer sandwich structure using Ethylene-vinyl acetate (EVA) between thin Aluminum plates to limit localized deformation of the structure, yet capable of propagating the necessary strain on the FBG to cause spectrum shift. EVA is a form of rubber, typically found in shoe soles. These are inexpensive, lightweight, and have mechanical properties suitable for this application. The structure should be standing on rigid solid steel frames to maximize support. The fiber should be passing through the bottom region of the EVA.

Gauge 24 Aluminum Sheets of 0.511mm thickness with a 39.18 mm EVA layer, supported by 35mm width ASTM A36 steel bar showed optimum deformation in the applied range of force. The platforms overall length and width were chosen to be 0.8m and 0.4m respectively.

Figure 15 and Figure 16 illustrates the described geometry, and Table 12-1 shows the mechanical properties of the materials used.

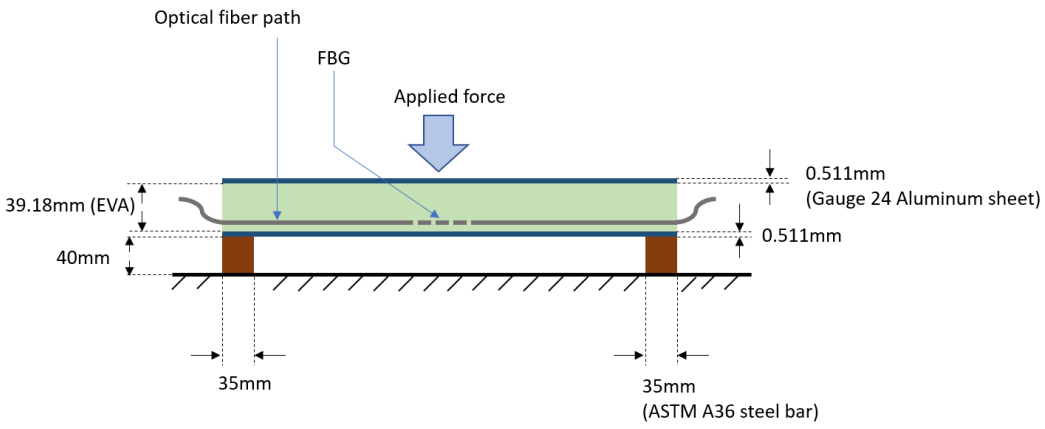

Figure 15 Physical Design of the force platform (cross-section, not to scale)

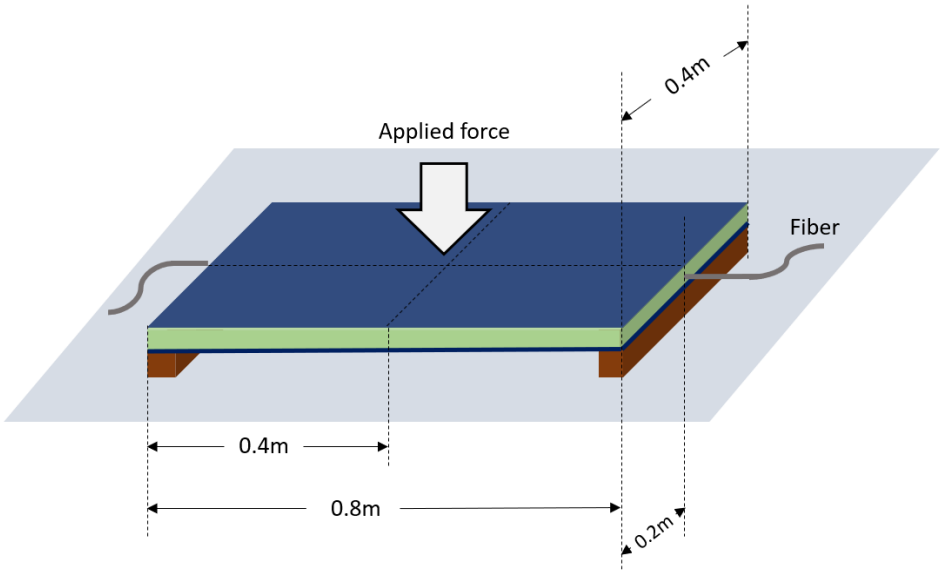

Figure 16 Physical Design of the force platform (3D-view, not to scale)

12.3.1.2 Mechanical Properties

Mechanical properties are shown in Table 12-1.

Table 12-1 Mechanical properties of the materials in the force platform

Part	**Material**	**Young Modulus**	**Poisson Ratio**
Top and Bottom layers	Gauge 24 Aluminum Sheet	73.1 GPa	0.33
Middle layer	Ethylene-vinyl acetate (EVA)	0.01 GPa	0.48
Support frame	ASTM A36 Steel Bar	200GPa	0.26

12.3.2 A stiff object to apply force on the platform

12.3.2.1 Geometry

A stiff body is required to apply force onto the platform surface. A stiff body is constructed keeping similarity with a human foot/prosthetic limb's dimensions. Mechanical properties of human bone

are used. It should be noted that we could use any rigid body to apply force on the platform, the final results of our interest are independent of this body's shape as long as we have a curved surface to apply the pressure on the platform, and which is rigid enough to not getting severely deformed itself. This body is constructed to emulate a human foot closely mainly in terms of contact surfaces, and material elastic properties. The dimensions and mechanical properties of this rigid body is given in Figure 17.

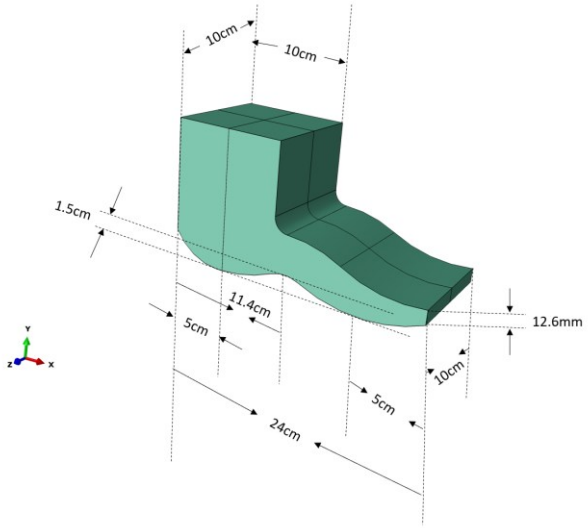

Figure 17 Dimensions of the stiff body used to apply pressure on the platform

12.3.2.2 Mechanical Properties

Mechanical properties of this pressure applying object are listed in Table 12-2 :

Table 12-2 Mechanical Properties of stiff object used to apply force on the platform

Part	**Material**	**Young modulus**	**Poisson Ratio**
Stiff object to apply force on the platform	Human bone	7.3 GPa	0.3

12.4 FEM Model (Abaqus CAE)

An FEM model for the force platform including the force applying object was developed in Abaqus CAE. There are multiple stages of developing an FEM model in Abaqus, including geometry, material properties, assembly, step (analysis process), interaction properties, loading and meshing. These stages, and attributes used in this simulation are summarized in Table 12-3:

Table 12-3 Summary of FEM Modeling Stages in Abaqus CAE

Stage		**Details**
Mechanical Structure		Dimensions as in Figure 15, Figure 16 and Figure 17.
Properties	Material properties	As described in Table 12-1 and Table 12-2
	Section Assignments	As described in Figure 15
	Composite Layup	Corresponding to dimensions in Figure 15, the composite layup is shown in Figure 18
Assembly		Coincident points were used to constrain the bottom point of the heel to the surface of the platform.
Step		Type: Static, General Nlgeom = ON (Nlgeom is turned on to account for geometric nonlinearities in the system and to handle large deformations if any)
Interaction	Type	Standard surface to surface contact
	Master/Slave	Master surface: Bottom of the foot (stiffer) Slave surface: Top surface of the platform

	Properties	Tangential Behavior	Penalty; Friction Coefficient: 0.5
		Normal Behavior	Hard Contact
	Constraint type	Tie	
Load	Boundary Conditions	Encastre at the bottom surface of the support steel bar. No movement in any direction. Figure 19	
	Load	Uniform pressure calculated from the force and the area it is applied on. (500N - 8000N)	
Mesh		Mesh on instance: Hex Global seed: Approximate global size 0.005 Illustration on Figure 20	

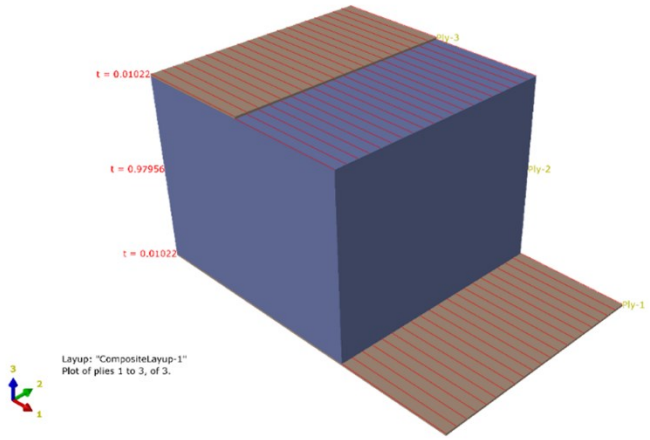

Figure 18 Composite Layup in Abaqus CAE

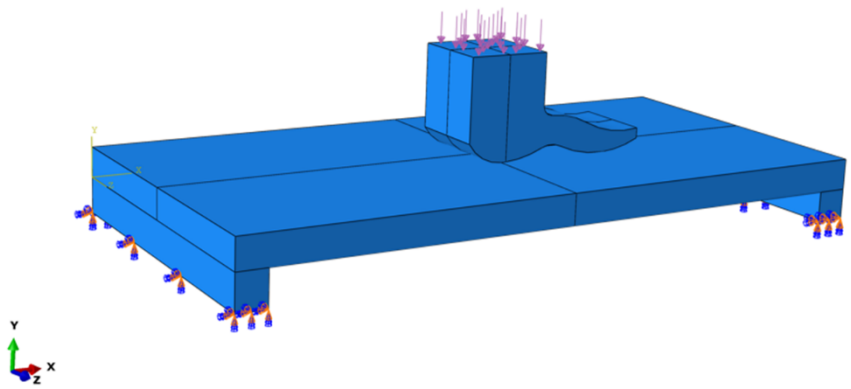

Figure 19 Mechanical Assembly in Abaqus CAE

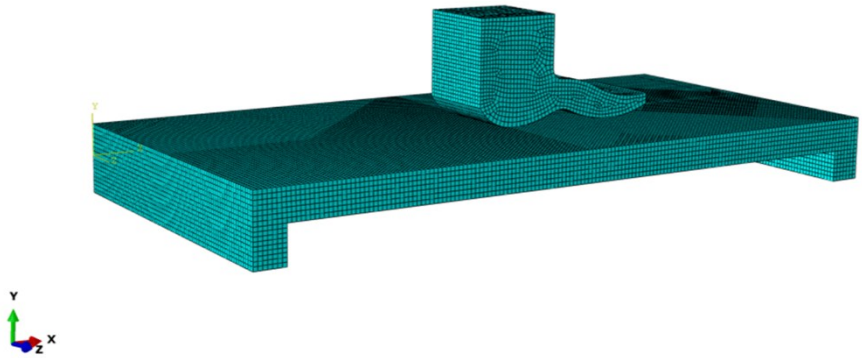

Figure 20 Meshing of the assembled structure in Abaqus CAE

12.5 FEA Results

12.5.1 Strain Distribution and Deformation (Displacement)

The logarithmic strain distribution throughout the force platform structure for 8000N (1000N margin is kept from 7000N requirement) applied force on the top surface of the stiff object is shown Figure 21 and Figure 22 from two viewpoints. We can initially observe that the maximum strain in the x direction (along the fiber) irrespective of location is $5.6 \times 10^{-3}\epsilon$, which is approximately half of the typical FBG strain tolerance of $10^{4}\mu\epsilon$, as described in section 12.2. We would also observe that the maximum strains are at the bottom surface of the platform along the center where the force was applied.

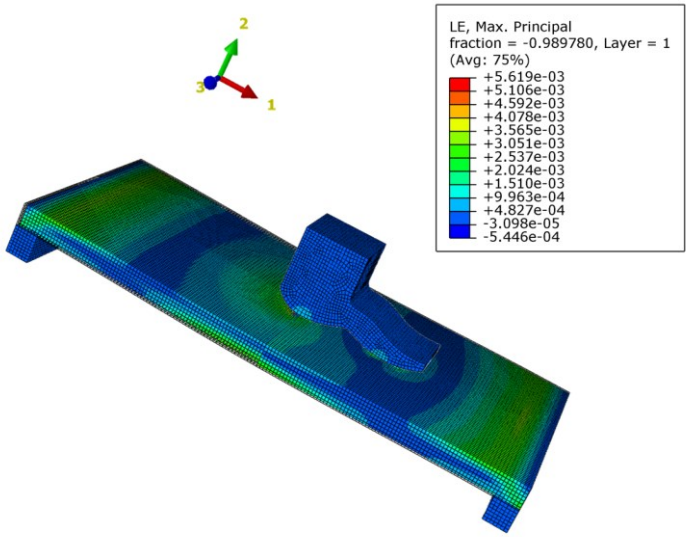

Figure 21 Strain distribution at 8000N force (view 1)

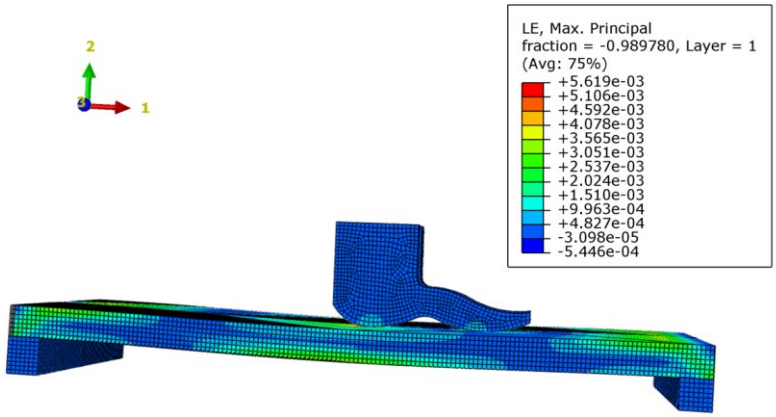

Figure 22 Strain distribution at 8000N force (view 2)

The displacement along the 3 axes at the central bottom surface were found to be: -5.03721×10^{-5} along X axis, -6.57475×10^{-3} along Y axis or the direction of the force applied, and -6.50042×10^{-6} along the Z axis.

There is only 6.57 mm of deformation along the vertical axis and micrometer range (negligible) deformation along the other two axes, which are certainly in the acceptable range. Since the platform depth is 5cm, so maximum deformation displacement is 1.3% at 8000N.

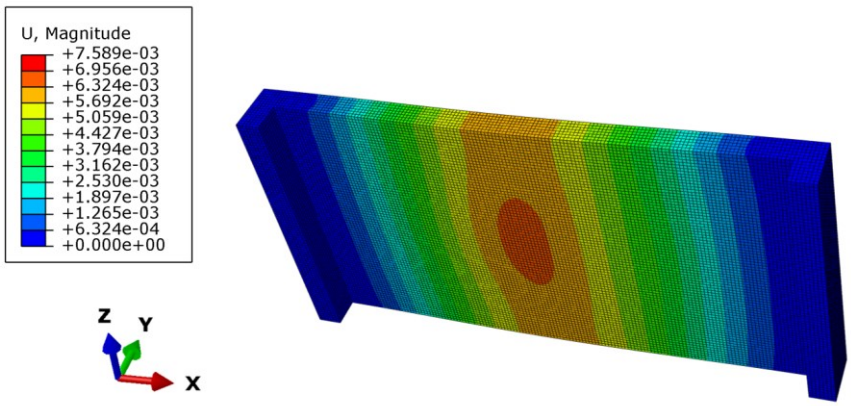

Figure 23 Displacement/deformation at 8000N force

13 FBG Spectrum Simulation from FEA Results Data

13.1 Choosing the fiber path

From the FEM visualization, it was qualitatively observed that longitudinal strain is more evenly distributed at the bottom region of the plate along to the applied force direction. To precisely understand a favorable location for the gratings, we looked at the strain distribution along 10 different fiber paths starting from 5 mm above the aluminum layer up-to 10 mm above it, each going across the platform one side to another through the middle. A few fiber paths are illustrated in Figure 24.

Path 1 being at 5mm distance, and path 10 at 14 mm, we get the following strain profile from 0.2m to 0.6m along the platform as shown in Figure 25. In this comparison, the applied force is kept constant at 5000N. This gives us a clear picture of where we could have our fiber path. Since Path 1, gives us maximum strain profile, we selected path 1 as a suitable fiber path for next steps of analysis.

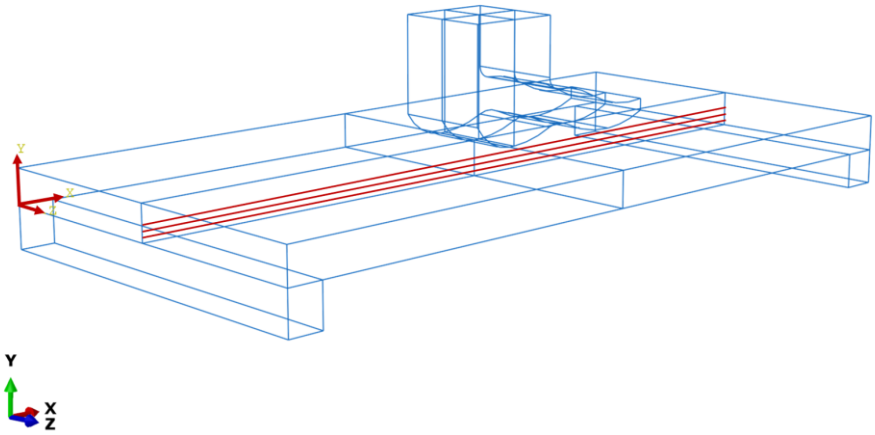

Figure 24 Illustrating the arrangement of the fiber test paths

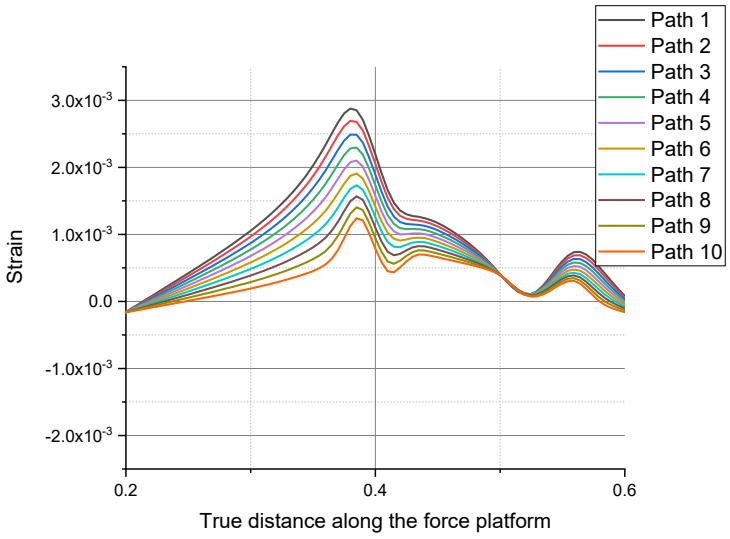

Figure 25 Strain along the fiber direction for 10 different paths from the bottom surface for 5000N

13.2 Setting the FBG Location

After selecting a suitable fiber path, the next step is to choose an FBG location at that path for further analysis. To do this, we fixed the fiber path in the last section, and then applied loads of 500 to 8000N on a 1000N interval. We get the following profile as shown in Figure 26 for varying loads:

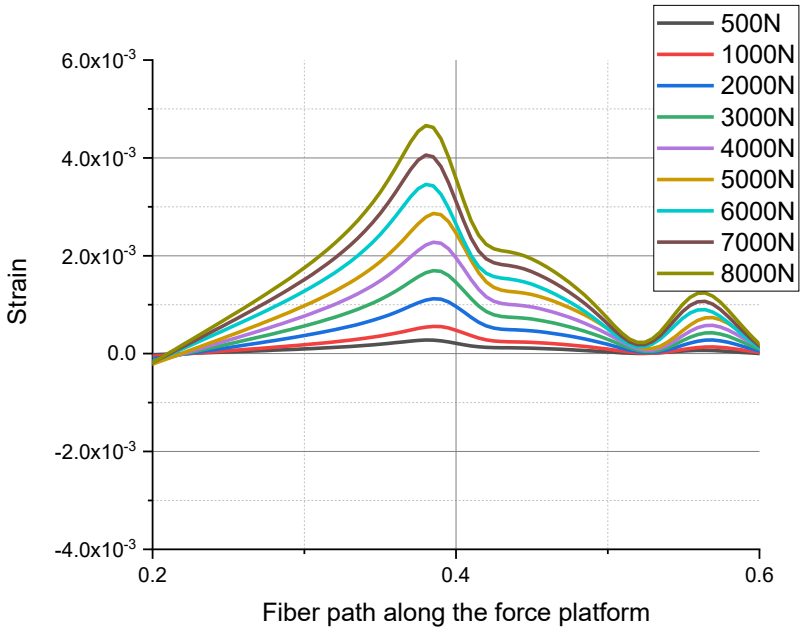

Figure 26 Strain along the chosen fiber path for varying loads

The maximum strain at the along the fiber path that was chosen in Section 13.1, was found to be less than close to 4600με near the location of the contact point of force applying body and the platform, caused by the maximum load of 8000N, and minimum was found to be 278 με caused by 500N of applied force. The maximum strain was found to be at 0.38m, the contact point of the heel and the platform.

It was mentioned earlier that standard FBGs can tolerate maximum of 10000 με, and our maximum strain is well within this range. Comparatively inexpensive wavelength meters can detect up-to 10pm precision. 278 με yields 0.338 nm wavelength shift, which is easily detectable in even low-end meters. OMM6810B wavelength meter with 0.1 nm resolution from Newport (www.newport.com/p/OMM-6810B-100V) costs USD 3,133, while a 0.1 pm resolution meter from Thorlabs (https://www.thorlabs.com/newgrouppage9.cfm?objectgroup_id=5276) costs USD 27,000-34,000.

The fiber and FBG locations were finalized to be:

Start point coordinate: $(3\times10^{-4},\ 5\times10^{-3},\ 0.2)$; **End point coordinate:** $(0.8,\ 5\times10^{-3},\ 0.2)$

FBG location: 0.38m from the start point.

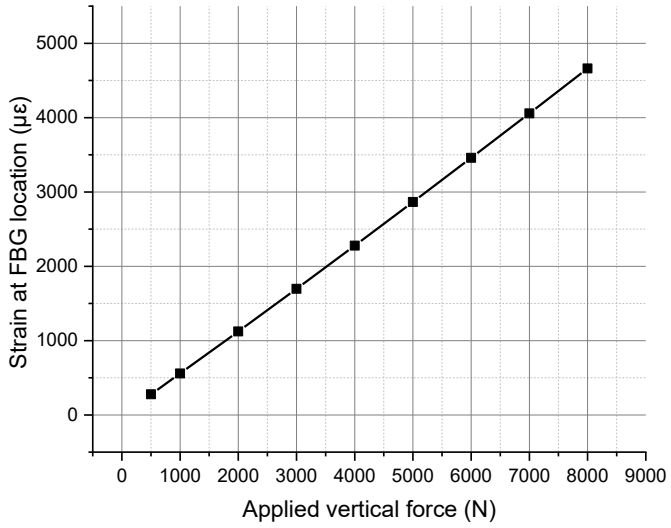

Figure 27 Force-Strain relationship at the chosen fiber path and FBG location

If we organize the strain values at the selected FBG location, along the selected fiber path, with respect to the varying applied forces, we get the relationship as shown in Figure 27. This nature of induced strain due to applied forces would also be reflected in the wavelength shift results.

13.3 Simulation Parameters

In this stage, we would use the results of the Abaqus FEM model to simulate the reflected spectrum shift from the FBG, if its parameters were chosen according to the suitable ranges found out in section 11 (parametric simulation), and if the FBG was located in the optimized location along the optimized path as found out in section 13.1 and section 13.2. Standard values were used for other parameters that are required to simulate the FBG reflected spectrum. The used parameters are listed in Table 13-1.

Table 13-1 Simulation Parameters: FBG reflected spectra under loading

Photo-elastic parameter, p_e		0.215
Initial effective refractive index, n_{eff}		1.46
Mean induced change in the refractive index, $\overline{\delta_{n_{eff}}}$		4.5×10^{-4}
Fringe visibility, fv		1.0
Directional Refractive index parameters:	p_{11}	0.121
	p_{12}	0.270
Young Modulus (Pa)		75×10^{9}
Poisson Ratio		0.17
FBG length (mm)		5
Original wavelength (nm)		1550

13.4 Simulation Results (FBG under static loads: birefringence ignored)

With the parameters as in Table 13-1, the FBG spectra are simulated. As expected, we observe the reflected spectra to shift with each increasing force load on the transducer. The spectrum shifts are illustrated in Figure 28. The effect of birefringence due to transverse stress is ignored in this stage to give a perspective on the evolution of only spectrum shift for increasing loads. The birefringence distortion will be discussed in the next section.

The spectrum shifts were calculated for each applied static load and shown in Figure 29. From a static analysis point of view, we find a linear relationship for the wavelength shift with respect to a realistic range of applied force on the transducer. This proves an initial feasibility of the designed transducer for this application.

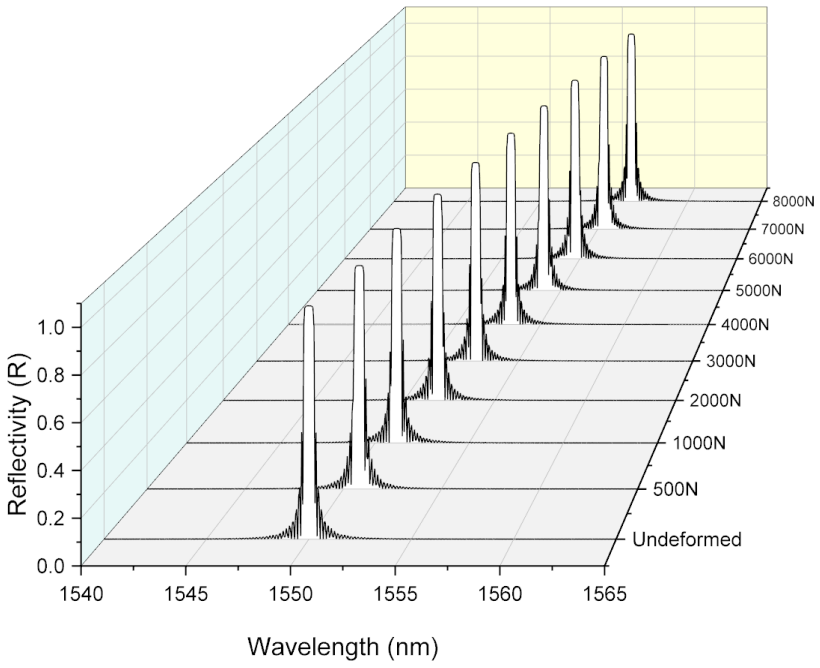

Figure 28 FBG Reflected Spectra for varying load on the platform: ignoring the effect of transverse stress (birefringence)

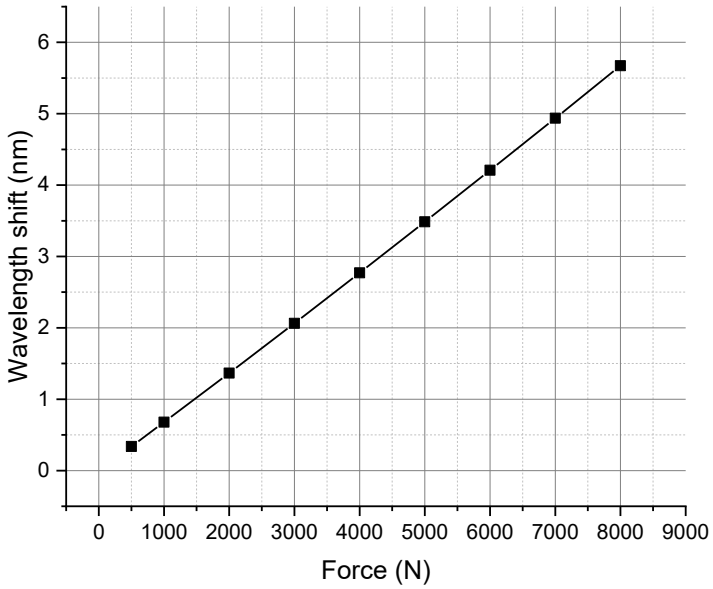

Figure 29 (FBG Reflected Spectra for varying load on the platform: ignoring the effect of transverse stress (birefringence); static analysis with realistic range of forces)

13.5 Simulation results (FBG under static load: including the effect of birefringence, i.e. peak splitting)

From the theory of birefringence, we know that due to applied transverse force, the stresses in the transducer cause two orthogonally polarized modes resulting in the reflected spectrum as being perceived to be split. The amount of split in the peaks being smaller compared to the spectrum width, they are perceived to be distorted, and the magnitude of the reflected spectrum tends to decrease. When we incorporate the birefringence calculations into the reflected spectrum results, we observe that the peaks start to strongly split with 6000N of applied force. The evolution of the reflected spectra after considering birefringence, for varying loads, is shown in Figure 30. To illustrate further, Figure 31 shows the effect of birefringence for the case of 5000N where we can particularly observe the Y and Z polarized waves contributing to the distorted final spectrum.

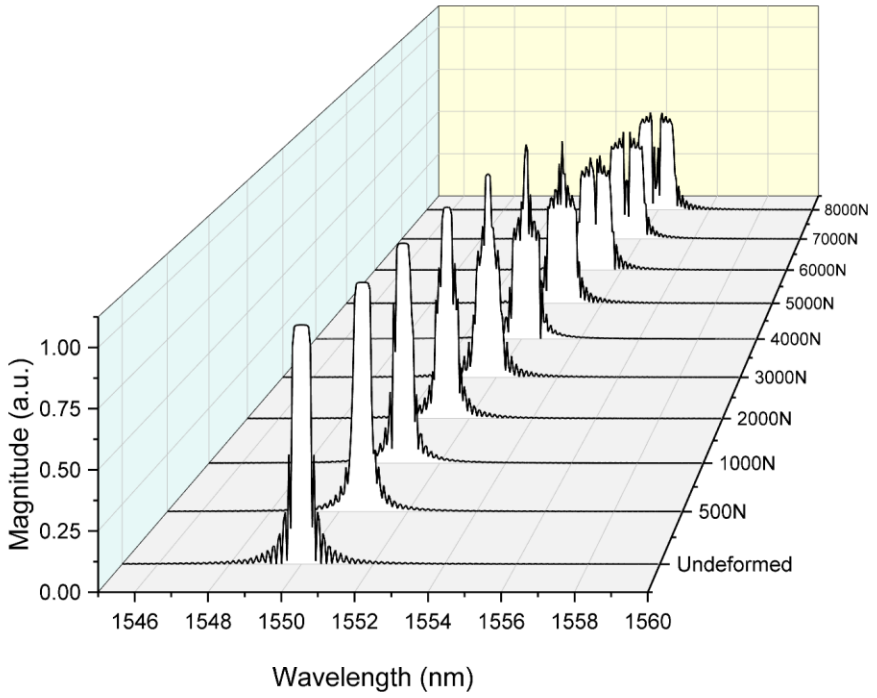

Figure 30 FBG reflected spectra for different static loads on the platform due to longitudinal strain and transverse stress (birefringence)

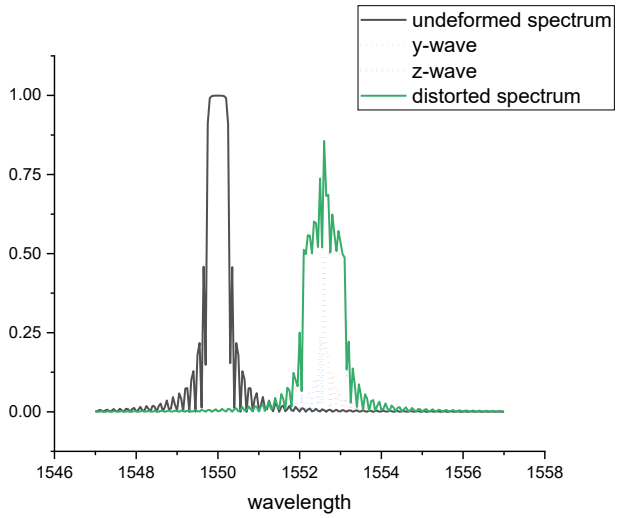

Figure 31 Snapshot of 5000N from the FBG reflected spectra illustrating birefringence

If we calculate the width variation of the split spectra according to equation (17), we find that it is not significant with respect to the actual wavelength shifts that we obtain due to longitudinal strain along the fiber. The width variation always remains within 15% of the wavelength shift for each case (applied load). For comparison, the wavelength shift and the width variation are both shown at the same scale in Figure 32.

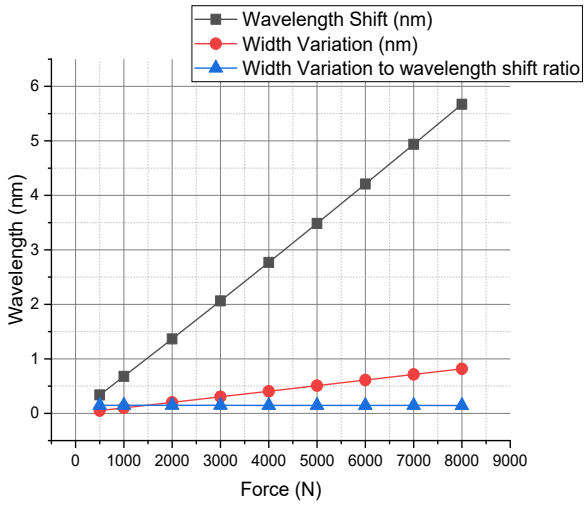

Figure 32 Comparison of wavelength shift (due to strain) and width variation (due to birefringence) on the same scale

From the slope of our wavelength shift vs force applied results, we find a sensitivity of 0.711pm/N. This means that with an inexpensive 10pm resolution wavelength meter, we can expect to measure forces with a precision of approximately 15N, which is equivalent of a 1.5Kg mass.

13.6 Comparing the results

The dependence of wavelength shift with respect to force applied on the transducer depends on how the structure is deformed and induces longitudinal strain along the fiber. Since, the design of this transducer is novel, it is not possible to directly compare the force vs wavelength shift results of this study with literature. However, the accuracy of the FBG spectrum simulation itself can be verified from literature. Zhang et al's [35] experimental work on FBGs dealt with strain ranges comparable to the strain range we have used here, i.e. the corresponding induced strain range at the FBG location caused by the applied range of forces on the transducer. Zhang's setup involved applying axial strain directly to the FBG using a cryogenic box setup. Zhang et al also used similar fiber and FBG parameters that were used in our work. Comparing the strain vs wavelength shift of this work to our results, we observe a very good match.

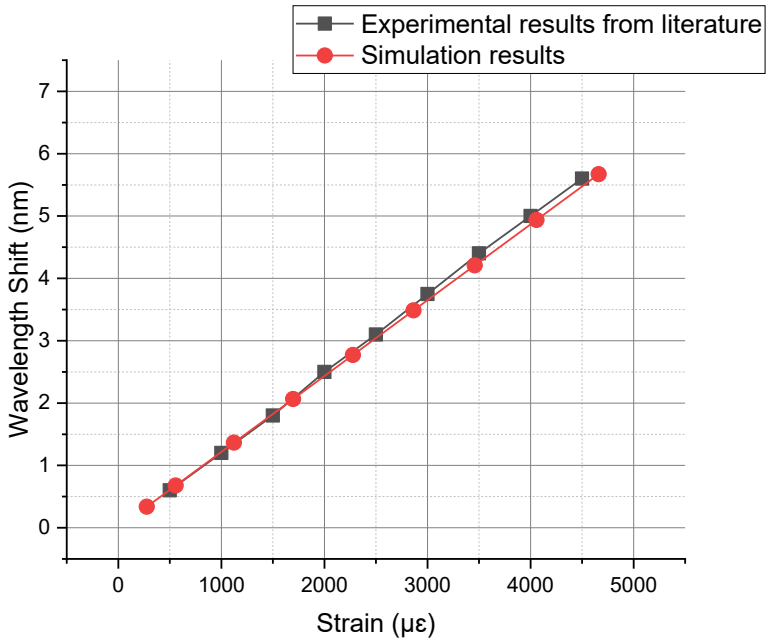

Figure 33 Comparing the strain vs wavelength shift results with Zhang et al's work in [35]

Chapter 4
Conclusion

14 Concluding Remarks

We have proved that it is feasible to use Fiber Bragg Grating (FBG) based strain sensors for higher range of force sensing applications, such as in a biomechanical force platform, by designing a transducer capable of translating vertical force into longitudinal strain that would act on the FBG. We used theoretical models in the literature and established properties of FBGs to systematically analyze the possibilities and complexities of using FBGs in such an application. We have proposed and simulated the transducer (force platform) and shown that it can measure realistic ranges of forces for this application. We have also analyzed the intrinsic practical limitations of FBGs, e.g. birefringence and elaborated on how we can choose FBG fabrication parameters for optimum results. We found a suitable range of FBG length and modulation depth which are reasonable in this application. We also observed their evolution. We designed a simplified transducer able to measure external transverse force by inducing longitudinal strain in a range that the fiber can easily withstand.

15 Limitations and Future Works

The purpose of this work was the quantitative evaluation of the feasibility of using FBGs in higher range force sensing. From a mathematical modeling point of view, the effect of using an apodized/chirped model for the grating can be an interesting extension of this work. Apodization of a grating means having a non-uniform refractive index profile, typically gaussian or a raised cosine, which improves side lobe suppression while maintaining high reflectivity and a narrow band in the FBG reflected spectra [14]. From the transducer design point of view, The analysis in this work involved static mechanical forces. A more complex study of the transducer, such as a dynamic analysis based on the time dependent characteristic of a force sensing application, such as gait, impact etc. are mechanical engineering problems, and hence out of scope of this study and suggested as a future work. Therefore, an immediate next step of this study could be an in-depth dynamic analysis for the response of the proposed force platforms, and later, a physical implementation of it and testing the results.

Bibliography

[1] H. Xiao *et al.*, “Optical fiber sensors for high temperature harsh environment applications,” *Proc. SPIE*, vol. 7647, pp. 76470U 1–15, 2010.

[2] S. J. Mihailov, “Fiber Bragg Grating Sensors for Harsh Environments,” pp. 1898–1918, 2012.

[3] R. Pirich and K. D. Ambrosio, “Fiber Optics for Harsh Environments,” 2011.

[4] E. Udd and W. Spillman Jr, *Fiber Optic Sensors: An Introduction for Engineers and Scientists*. John Wiley and Sons Inc, 2011.

[5] Clean Energy Institute- University of Washington, “No Title.” [Online]. Available: https://www.cei.washington.edu/education/science-of-solar/battery-technology/. [Accessed: 13-Jul-2018].

[6] K. Iyer, “Development of Multifunctional Fiber Optic Sensors for Lithium Ion-Battery Monitoring by,” 2016.

[7] H. Guo, G. Xiao, N. Mrad, and J. Yao, “Fiber optic sensors for structural health monitoring of air platforms,” *Sensors*, vol. 11, no. 4, pp. 3687–3705, 2011.

[8] S. Šprager, D. Donlagić, and D. Zazula, “Monitoring of basic human vital functions using optical interferometer,” *Int. Conf. Signal Process. Proceedings, ICSP*, pp. 1738–1741, 2010.

[9] S. Šprager and D. Zazula, “Detection of heartbeat and respiration from optical interferometric signal by using wavelet transform,” *Comput. Methods Programs Biomed.*, vol. 111, no. 1, pp. 41–51, Jul. 2013.

[10] F. C. Favero, J. Villatoro, and V. Pruneri, “Microstructured optical fiber interferometric breathing sensor,” *J. Biomed. Opt.*, vol. 17, no. 3, p. 037006, Mar. 2012.

[11] M. Fajkus, J. Nedoma, R. Martinek, V. Vasinek, H. Nazeran, and P. Siska, “A Non-Invasive Multichannel Hybrid Fiber-Optic Sensor System for Vital Sign Monitoring,” *Sensors*, vol. 17, no. 12, p. 111, Jan. 2017.

[12] E. Schena, D. Tosi, P. Saccomandi, E. Lewis, and T. Kim, “Fiber Optic Sensors for Temperature Monitoring during Thermal Treatments: An Overview,” *Sensors*, vol. 16, no. 7, p. 1144, Jul. 2016.

[13] L. Dziuda, “Fiber-optic sensors for monitoring patient physiological parameters: a review of applicable technologies and relevance to use during magnetic resonance imaging procedures,” *J. Biomed. Opt.*, vol. 20, no. 1, p. 010901, Jan. 2015.

[14] R. Kashyap, “Principles of Optical Fiber Grating Sensors,” *Fiber Bragg Gratings*, pp. 441–502, 2009.

[15] V. Bhatia, D. Campbell, R. O. Claus, and A. M. Vengsarkar, “Simultaneous strain and temperature measurement with long-period gratings,” *Opt. Lett.*, vol. 22, no. 9, p. 648, 2008.

[16] M. J. Kim, Y. H. Kim, G. Mudhana, and B. H. Lee, “Simultaneous measurement of temperature and strain based on double cladding fiber interferometer assisted by fiber grating pair,” *IEEE Photonics Technol. Lett.*, vol. 20, no. 15, pp. 1290–1292, 2008.

[17] L. Schenato, *A Review of Distributed Fibre Optic Sensors for Geo-Hydrological Applications*, vol. 7, no. 9. 2017.

[18] B. H. Lee *et al.*, “Interferometric fiber optic sensors,” *Sensors*, vol. 12, no. 3, pp. 2467–2486, 2012.

[19] P. Roriz and A. B. Lobo Ribeiro, *Fiber Optical Sensors in Biomechanics*. Elsevier Inc., 2018.

[20] Wikipedia contributors, “No Title.” [Online]. Available: https://en.wikipedia.org/wiki/Force_platform. [Accessed: 12-Aug-2018].

[21] M. G. Silva, P. V. S. Moreira, and H. M. Rocha, “Development of a low cost force platform for biomechanical parameters analysis,” *Res. Biomed. Eng.*, vol. 33, no. 3, pp. 259–268, 2017.

[22] P. Roriz, L. Carvalho, O. Frazão, J. L. Santos, and J. A. Simões, “From conventional sensors to fibre optic sensors for strain and force measurements in biomechanics applications: A review,” *J. Biomech.*, vol. 47, no. 6, pp. 1251–1261, 2014.

[23] Y. Ma *et al.*, “High Sensitive Z-shaped Fiber Interferometric Refractive Index Sensor: Simulation and Experiment,” *IEEE Photonics Technol. Lett.*, vol. 30, no. 12, pp. 1131–1134, 2018.

[24] H. Hochreiner, M. Cada, and P. D. Wentzell, “Modeling the response of a long-period fiber grating to ambient refractive index change in chemical sensing applications,” *J. Light. Technol.*, vol. 26, no. 13, pp. 1986–1992, 2008.

[25] H. Hochreiner, M. Cada, and P. D. Wentzell, “Tuning the response of long-period fiber gratings for chemical sensing applications,” vol. 6765, no. 902, pp. 1–15, 2007.

[26] L. Long, “Multi-axis fiber bragg grating accelerometer,” 2010.

[27] M. Yamada and K. Sakuda, “Analysis of almost-periodic distributed feedback slab waveguides via a fundamental matrix approach,” *Appl. Opt.*, vol. 26, no. 16, p. 3474, Aug. 1987.

[28] K. Peters, M. Studer, J. Botsis, A. Iocco, H. Limberger, and R. Salathé, “Embedded optical fiber Bragg grating sensor in a nonuniform strain field: Measurements and simulations,” *Exp. Mech.*, vol. 41, no. 1, pp. 19–28, Mar. 2001.

[29] H.-Y. Ling, K.-T. Lau, W. Jin, and K.-C. Chan, “Characterization of dynamic strain measurement using reflection spectrum from a fiber Bragg grating,” *Opt. Commun.*, vol. 270, no. 1, pp. 25–30, Feb. 2007.

[30] Y. Chen, J. Li, Y. Yang, M. Chen, J. Li, and H. Luo, “Numerical modeling and design of mid-infrared FBG with high reflectivity,” *Optik (Stuttg).*, vol. 124, no. 16, pp. 2565–2568, 2013.

[31] G. Pereira, M. McGugan, and L. P. Mikkelsen, “FBG_SiMul V1.0: Fibre Bragg grating signal simulation tool for finite element method models,” *SoftwareX*, vol. 5, pp. 163–170, Jan. 2016.

[32] G. F. Pereira, L. P. Mikkelsen, and M. McGugan, “Crack Detection in Fibre Reinforced Plastic Structures Using Embedded Fibre Bragg Grating Sensors: Theory, Model Development and Experimental Validation,” *PLoS One*, vol. 10, no. 10, p. e0141495, Oct. 2015.

[33] O. Hassoon, M. Tarfoui, and a El Malk, “Numerical Simulation of Fiber Bragg Grating Spectrum for Mode-I Delamination Detection,” *Int. J. Mech. Aerospace, Ind. Mechatronics Eng.*, vol. 9, no. 1, pp. 144–149, 2015.

[34] S. Udoh, J. Njuguma, and R. Prabhu, “Modelling and simulation of fiber Bragg grating characterization for oil and gas sensing applications,” *First Int. Conf. Syst. Informatics, Model. Simul.*, pp. 213–218, 2014.

[35] X. Zhang, “Strain dependence of fiber Bragg grating sensors at low temperature,” *Opt. Eng.*, vol. 45, no. 5, p. 054401, 2006.

[36] D. Hu, L. Qin, Y. Guo, H. Liu, and J. Kong, “Design and Investigation of a Reusable Surface-mounted Optical Fiber Bragg Grating Strain Sensor,” *IEEE Sens. J.*, vol. 16, no. 23, pp. 1–1, 2016.

[37] J. H. Y.-Z. L. Y. C. H. B. K. N. Swee Chuan Tjin, Jianzhong Hao, Yu-, “A Pressure Sensor Using Fiber Bragg Grating,” *Fiber Integr. Opt.*, vol. 20, no. 1, pp. 59–69, Jan. 2001.

[38] Y. Zhao, H. Zhao, and J. Yang, “A novel weight measurement method based on birefringence in fiber Bragg gratings,” *Front. Optoelectron. China*, vol. 1, no. 3–4, pp. 226–230, 2008.

[39] J. Z. Hao *et al.*, “Design of a foot-pressure monitoring transducer for diabetic patients based on FBG sensors,” in *The 16th Annual Meeting of the IEEE Lasers and Electro-Optics Society, 2003. LEOS 2003.*, vol. 1, pp. 23–24.

[40] A. G. Leal-Junior, A. Frizera, L. M. Avellar, C. Marques, and M. J. Pontes, “Polymer Optical Fiber for In-Shoe Monitoring of Ground Reaction Forces during the Gait,” *IEEE Sens. J.*, vol. 18, no. 6, pp. 2362–2368, 2018.

[41] R. Correia, S. James, S. W. Lee, S. P. Morgan, and S. Korposh, “Biomedical application of optical fibre sensors,” *J. Opt. (United Kingdom)*, vol. 20, no. 7, 2018.

[42] J. L. Santos, A. B. Lobo-Ribeiro, P. Roriz, O. Frazão, and J. A. Simões, “Review of fiber-optic pressure sensors for biomedical and biomechanical applications,” *J. Biomed. Opt.*, vol. 18, no. 5, p. 050903, 2013.

[43] C. C. E. Campanella, A. Cuccovillo, C. C. E. Campanella, A. Yurt, and V. M. N. Passaro, “Fibre Bragg Grating based strain sensors: Review of technology and applications,” *Sensors (Switzerland)*, vol. 18, no. 9, 2018.

[44] H. Hu, S. Li, J. Wang, Y. Wang, and L. Zu, “FBG-based real-time evaluation of transverse cracking in cross-ply laminates,” *Compos. Struct.*, vol. 138, no. 138, pp. 151–160, Mar. 2016.

[45] X. Qiao, Z. Shao, W. Bao, and Q. Rong, “Fiber bragg grating sensors for the oil industry,” *Sensors (Switzerland)*, vol. 17, no. 3, 2017.

[46] R. Huq and M. Cada, “Fiber Bragg Gratings for Force Sensing in Biomechanics Applications,” submitted to: *Sensors*, 2019.

[47] J. Van Roey, J. Van Der Donk, and P. E. Lagasse, “Beam-propagation method : analysis and assessment Ear) = JJJ,” vol. 71, no. 7, 1981.

[48] K. Peters *et al.*, “Embedded optical fiber Bragg grating sensor in a nonuniform strain field: Measurements and simulations,” *Exp. Mech.*, vol. 41, no. 1, pp. 19–28, Mar. 2006.

[49] A. Bertholds and R. Dandliker, “Determination of the individual strain-optic coefficients in single-mode optical fibres,” *J. Light. Technol.*, vol. 6, no. 1, pp. 17–20, 1988.

[50] A. Ikhlef, R. Hedara, and M. Chikh-bled, “Uniform Fiber Bragg Grating modeling and simulation used matrix transfer method,” *IJCSI Int. J. Comput. Sci.*, vol. 9, no. 1, pp. 368–374, 2012.

[51] W. Zhang, W. Chen, Y. Shu, X. Lei, and X. Liu, “Effects of bonding layer on the available strain measuring range of fiber Bragg gratings,” *Appl. Opt.*, vol. 53, no. 5, p. 885, 2014.